Molecular Cell

Article

EXO1 protects BRCA1-deficient cells against toxic DNA lesions

Graphical abstract

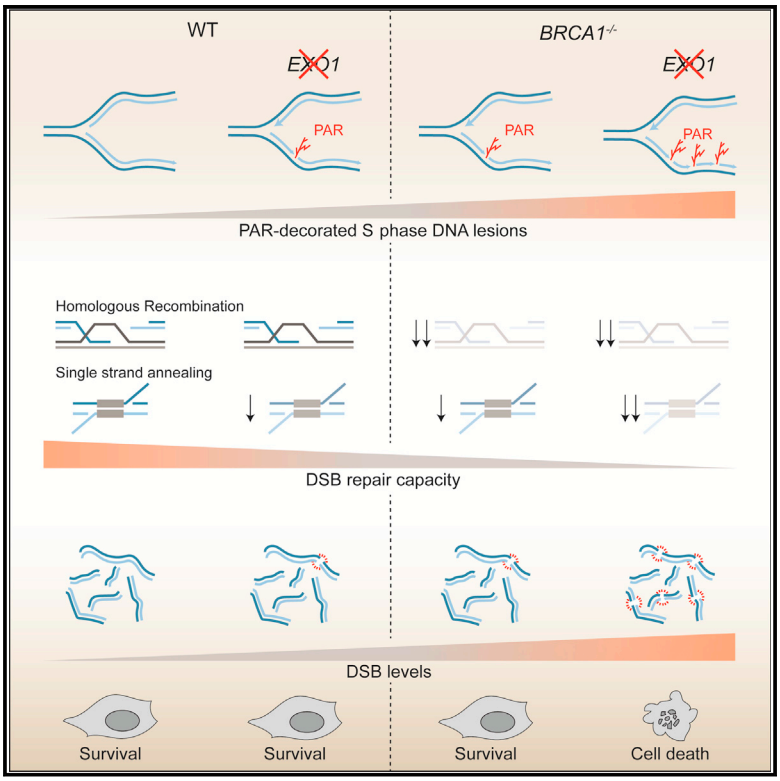

Highlights

- EXO1 is essential for the survival of BRCA1- but not BRCA2-deficient cells
- EXO1 loss induces S phase PAR signaling in both BRCA1- and BRCA2-deficient cells
- EXO1 loss causes toxic DNA double-strand break accumulation in BRCA1-deficient cells
- The double-strand break accumulation is caused by impaired single-strand annealing

Authors

Bert van de Kooij, Anne Schreuder, Raphael Pavani, ..., André Nussenzweig, Haico van Attikum, Sylvie M. Noordermeer

Correspondence

h.van.attikum@lumc.nl (H.v.A.), s.m.noordermeer@lumc.nl (S.M.N.)

In brief

van de Kooij et al. identify loss of the exonuclease EXO1 as a vulnerability of BRCA1-deficient cells. Mechanistically, cells deficient for both BRCA1 and EXO1 suffer from unrepaired DNA double-stranded breaks due to the loss of two break repair pathways, homologous recombination, and single-strand annealing.

van de Kooij et al., 2024, Molecular Cell *84*, 659–674
February 15, 2024 © 2023 The Authors. Published by Elsevier Inc.
https://doi.org/10.1016/j.molcel.2023.12.039

CellPress

Molecular Cell

CellPress
OPEN ACCESS

Article

EXO1 protects BRCA1-deficient cells against toxic DNA lesions

Bert van de Kooij,[1,2,8] Anne Schreuder,[1,3,8] Raphael Pavani,[4,8] Veronica Garzero,[1,3] Sidrit Uruci,[1] Tiemen J. Wendel,[1,3] Arne van Hoeck,[3,5] Marta San Martin Alonso,[1,3] Marieke Everts,[2] Dana Koerse,[1] Elsa Callen,[4] Jasper Boom,[6] Hailiang Mei,[6] Edwin Cuppen,[3,5,7] Martijn S. Luijsterburg,[1] Marcel A.T.M. van Vugt,[2] André Nussenzweig,[4] Haico van Attikum,[1,*] and Sylvie M. Noordermeer[1,3,9,*]

[1]Department of Human Genetics, Leiden University Medical Centre, Leiden 2333 ZC, the Netherlands
[2]Department of Medical Oncology, University Medical Center Groningen, Groningen 9713 GZ, the Netherlands
[3]Oncode Institute, Utrecht 3521 AL, the Netherlands
[4]Laboratory of Genome Integrity, National Cancer Institute, National Institutes of Health, Bethesda, MD 20892, USA
[5]Centre for Molecular Medicine, University Medical Centre Utrecht, Utrecht 3584 CG, the Netherlands
[6]Sequencing Analysis Support Core, Leiden University Medical Centre, Leiden 2333 ZC, the Netherlands
[7]Hartwig Medical Foundation, Amsterdam 1098 XH, the Netherlands
[8]These authors contributed equally
[9]Lead contact
*Correspondence: h.van.attikum@lumc.nl (H.v.A.), s.m.noordermeer@lumc.nl (S.M.N.)
https://doi.org/10.1016/j.molcel.2023.12.039

SUMMARY

Inactivating mutations in the *BRCA1* and *BRCA2* genes impair DNA double-strand break (DSB) repair by homologous recombination (HR), leading to chromosomal instability and cancer. Importantly, BRCA1/2 deficiency also causes therapeutically targetable vulnerabilities. Here, we identify the dependency on the end resection factor EXO1 as a key vulnerability of BRCA1-deficient cells. EXO1 deficiency generates poly(ADP-ribose)-decorated DNA lesions during S phase that associate with unresolved DSBs and genomic instability in BRCA1-deficient but not in wild-type or BRCA2-deficient cells. Our data indicate that BRCA1/EXO1 double-deficient cells accumulate DSBs due to impaired repair by single-strand annealing (SSA) on top of their HR defect. In contrast, BRCA2-deficient cells retain SSA activity in the absence of EXO1 and hence tolerate EXO1 loss. Consistent with a dependency on EXO1-mediated SSA, we find that *BRCA1*-mutated tumors show elevated *EXO1* expression and increased SSA-associated genomic scars compared with BRCA1-proficient tumors. Overall, our findings uncover EXO1 as a promising therapeutic target for BRCA1-deficient tumors.

INTRODUCTION

High fidelity repair of DNA double-strand breaks (DSBs) is essential for maintaining genomic integrity and preventing the onset of diseases such as cancer. Cells are equipped with several pathways to repair DSBs with varying fidelity. Homologous recombination (HR) is considered the most faithful type of repair. Loss of HR by disrupting mutations in core HR factors, such as BRCA1, BRCA2, and PALB2, is observed in many tumors of different origins and results in a distinct pattern of base substitutions, mutations, and rearrangements.[1–3] Furthermore, hereditary heterozygous mutations in these genes predispose to breast, ovarian, and prostate cancer.[4] Besides causing tumor formation, HR deficiency also provides vulnerabilities that can be exploited for anti-cancer therapy. The reduced capacity of HR-deficient tumors to maintain genomic stability renders them sensitive to drugs that damage DNA, such as platinum compounds or PARP inhibitors (PARPi).[5] Unfortunately, cancer cells frequently acquire resistance to these types of drugs.[6] This indicates a necessity to develop additional single-drug or combinatorial therapies.

To enable repair of DSBs by HR, the flanking DNA needs to be resected to expose stretches of single-stranded DNA (ssDNA). The ssDNA is then bound by the core HR-factor RAD51, which facilitates the search for an intact homologous sequence, most frequently the sister chromatid, that is subsequently invaded and functions as a template for repair. BRCA1 plays a role in multiple steps during HR. It facilitates RAD51 loading onto the resected DNA by recruitment of PALB2-BRCA2 and direct interaction with RAD51[7,8], and it stimulates the upstream process of DNA end resection,[9–11] although the extent of the resection defect upon BRCA1 loss seems to depend on the cellular model.[12–14]

End resection is initiated by the short-range end resection factors, MRE11 and CTIP, that remove up to 300 nucleotides of

This is an open access article under the CC BY-NC-ND license (http://creativecommons.org/licenses/by-nc-nd/4.0/).

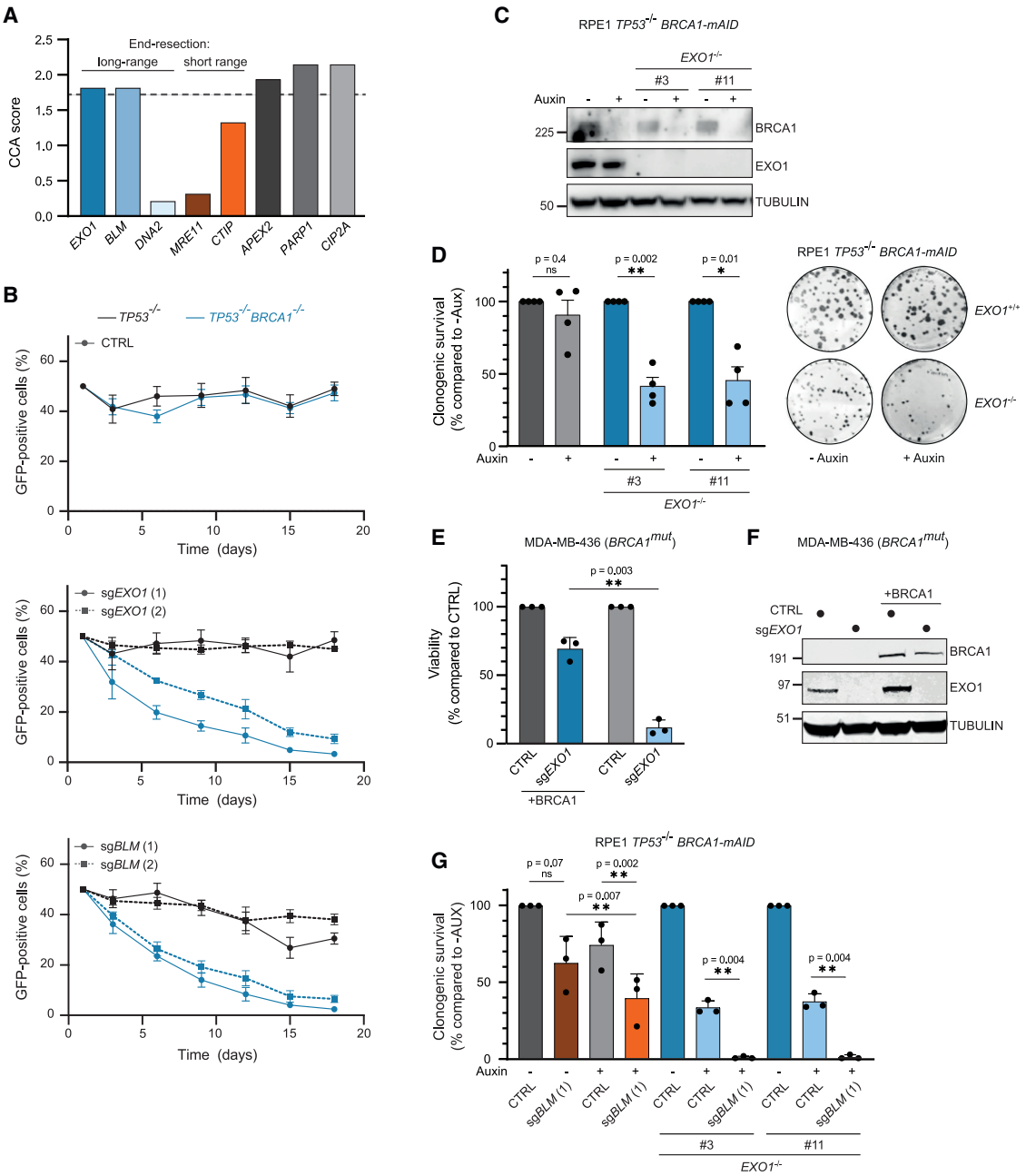

Figure 1. EXO1 loss is synthetically lethal with BRCA1 deficiency

(A) Selected results of a gene essentiality screen in BRCA1-proficient and -deficient RPE1 cells.[41] Plotted is the CCA score: a higher score indicates a unique essentiality in BRCA1-deficient cells compared with -proficient cells. Dashed line indicates the cut-off for a significant CCA score (based on Adam et al.[41]).

(B) RPE1 hTERT cells expressing Cas9, either *TP53*$^{-/-}$ (black lines) or *TP53*$^{-/-}$ *BRCA1*$^{-/-}$ (blue lines), were infected with indicated sgRNA together with GFP, or with an empty vector together with mCherry. GFP- and mCherry-positive cells were mixed 1:1, and the frequency of GFP-positive cells in the population was determined at multiple time points (n = 4, mean ± SEM). Western blot of lysates shown in Figure S1A.

(C) RPE1 hTERT *PAC*$^{-/-}$ *TP53*$^{-/-}$ cells were genetically modified to generate a BRCA1-mAID-GFP fusion gene at the endogenous *BRCA1* locus. In this genetic background, two clonal *EXO1*$^{-/-}$ cell lines were generated. Cells were treated with auxin (500 μM) for 48 h or left untreated, and lysates were analyzed by western blotting.

(D) The cell lines described in (C) were treated with 500 μM auxin, or left untreated, and clonogenic survival was determined. Right panel shows a representative experiment, left panel shows the quantification (n = 4, mean + SEM, ns = p > 0.05, *p < 0.05, **p < 0.01, paired t test).

(legend continued on next page)

ssDNA.[15] Long-range end resection subsequently can process thousands of nucleotides and is mediated either via the exonuclease EXO1 or the flap-endonuclease DNA2, which cooperates with the helicase BLM.[16] Interestingly, although short-range end resection is essential for HR, the role of long-range end resection is more enigmatic.[15,17,18] Several studies showed that long-range end resection plays a stimulatory role in HR and checkpoint activation,[19–21] whereas others have shown that HR is not affected by loss of long-range end resection proteins.[22–26]

In addition to HR, two other DSB repair pathways also depend on end resection: alternative end-joining (alt-EJ) and single-strand annealing (SSA). During alt-EJ, limited end resection is required to expose regions of microhomology flanking the DSB ends that anneal during repair, generally resulting in deletion of the intermittent sequence.[27–30] SSA requires more extensive long-range end resection to expose larger stretches of (imperfect) homology that can be located at distal regions up- and downstream of the DSB. The resected DNA is bound by RAD52 that drives annealing of the homologous regions, followed by the removal of the non-homologous intermittent ssDNA and subsequent repair by polymerases and ligases. Compared with alt-EJ, DSB repair by SSA generally leads to larger deletions.[7]

Although the contribution of SSA and alt-EJ to the repair of physiological DSBs in healthy cells is not fully understood, loss of either the alt-EJ factor POLQ or the SSA factor RAD52 is synthetically lethal with BRCA1 or BRCA2 loss.[28,31–33] This implies that DSB repair by alt-EJ or SSA is essential for survival of HR-deficient cells. However, recent studies suggested that increased ssDNA gap formation in the absence of POLQ may underlie the synthetic lethality with BRCA deficiency.[34–36] BRCA-deficient cells are prone to accumulate ssDNA gaps, and toxic levels of these lesions are associated with sensitivity to chemotherapy and PARPi.[37–40] Similarly, for RAD52, the synthetic lethal interaction with BRCA deficiency might not be driven by loss of SSA but rather by a potential function of RAD52 in BRCA-independent HR.[32,33]

To better understand the role of resection-driven DSB repair processes in BRCA-deficient cells, we studied the genetic interaction between end resection factors and BRCA deficiency. We show that long-range end resection mediated by EXO1 is essential for BRCA1-deficient cells, but not for BRCA2-deficient cells. Regardless of BRCA status, EXO1-loss results in poly(ADP-ribose) (PAR)-decorated DNA lesions. Our data suggest a model in which these lesions induce toxic genomic instability in cells that lack functional EXO1 and BRCA1 due to defective DSB repair by SSA, on top of their HR deficiency. In contrast, BRCA2-deficient cells retain high levels of end resection and SSA in the absence of EXO1 and therefore maintain genome stability. Thus, we uncover a novel vulnerability of BRCA1-deficient tumor cells and propose EXO1 as a novel therapeutic target for BRCA1-deficient tumors.

RESULTS

Long-range end resection factors are essential for BRCA1-deficient cells

A CRISPR screen that we performed previously, designed to identify essential genes in isogenic BRCA1-deficient versus BRCA1-proficient RPE1 cell lines,[41] allowed us to study the genetic interaction between BRCA1 and all end resection factors. As indicated by the high CCA score, the long-range end resection factors EXO1 and BLM were essential in BRCA1-deficient cells, but not in BRCA1-proficient cells, to a similar extent as previously described synthetic lethal interactors such as APEX2, PARP1, and CIP2A (Figure 1A).[42–44] In contrast to these long-range end resection factors, loss of the short-range end resection factors MRE11 and CTIP did not show significant synthetic lethal interactions with BRCA1 deficiency (Figure 1A). DNA2, another long-range end resection factor, was essential in both BRCA1-deficient and -proficient cells, in accordance with previous findings,[45–47] explaining its low CCA score (Figure 1A).

To validate these results, we performed competitive growth assays as described before.[48] In short, GFP-positive cells, depleted for the gene of interest, were mixed 1 to 1 with mCherry-positive control cells, and the composition of the mixed population was monitored over time. Confirming the results of the CRISPR screen, depletion of EXO1 or BLM by CRISPR-Cas9 strongly reduced the proliferation of BRCA1-deficient cells but not of BRCA1-proficient cells (Figures 1B and S1A). CTIP loss was toxic to both BRCA1-deficient and -proficient cells, although BRCA1-deficient cells seemed more sensitive to CTIP loss, as described previously.[49] Loss of MRE11 reduced the proliferation of both BRCA1-proficient and -deficient cells (Figures S1B and S1C). Together, these data indicate that short-range end resection is essential in all contexts, which is in agreement with previous reports.[50,51] In contrast, the long-range end resection factors EXO1 and BLM were essential only in a BRCA1-deficient background, calling for a better understanding of the role of these factors in this background.

To enable mechanistic studies on the synthetic lethal interaction between BRCA1 deficiency and loss of long-range end resection, we generated an RPE1 hTERT cell line containing an auxin-inducible degron (AID) fused to the endogenous *BRCA1* gene. This setup allowed us to deplete BRCA1 protein as fast as 2 h upon auxin treatment, resulting in strong PARPi sensitivity indicating functional BRCA1 loss (Figures S2A and S2B). Depletion of BRCA1 resulted in reduced levels of BARD1, its cognate heterodimer partner,[52] but did not affect the levels of BRCA2 and PALB2, validating our system as a BRCA1-specific depletion model (Figure S2A). In this background, we generated clonal *EXO1* knockout cell lines using CRISPR-Cas9 (Figure 1C). Corroborating the results of our competitive growth assays, EXO1 depletion only mildly affected the clonogenic survival of untreated BRCA1-proficient cells but strongly reduced cellular

(E) *BRCA1*-mutated MDA-MB-436 cells, either WT or reconstituted with BRCA1 cDNA, were infected with empty vector (CTRL) or *EXO1*-targeting sgRNA and viability was measured using CellTiter-Glo (n = 3, mean + SD, **p < 0.01, paired t test).
(F) Lysates of the MDA-MB-436 cell lines described in (E) were analyzed by western blotting.
(G) RPE1 hTERT *TP53*$^{-/-}$ BRCA1-mAID-GFP cell lines were virally transduced to express Cas9 cDNA and the indicated gRNAs, followed by a clonogenic survival assay in presence or absence of 500 μM auxin (n = 3, mean + SD, ns = p > 0.05, **p < 0.01 paired t test). Western blot of lysates shown in Figure S2K.

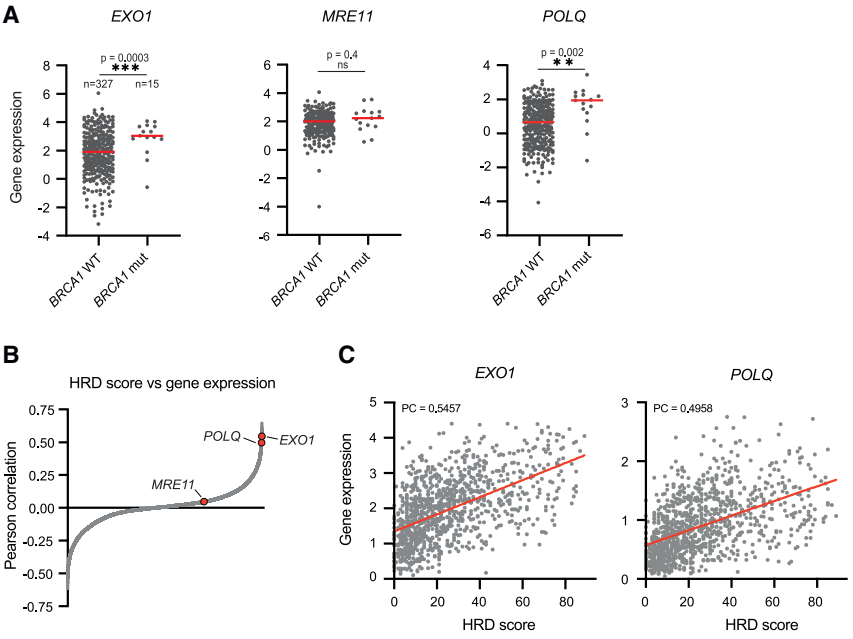

Figure 2. Elevated EXO1 expression in BRCA1-deficient tumors

(A) Gene expression of the indicated genes in *BRCA1* WT or mutant tumors of a breast cancer cohort[1] (red line indicates median, ns = $p > 0.05$, $^{**}p < 0.01$, $^{***}p < 0.001$, Kolmogorov-Smirnov).

(B) For breast cancer tumors of the TCGA cohort (n = 1,048), the correlation between the HRD score and expression level of an individual gene was determined. Plotted are the Pearson correlation coefficient for each of the 60,000 measured transcripts.

(C) HRD score and expression of the indicated genes were plotted for each tumor sample in the TCGA breast cancer dataset (n = 1,048). Red line is the linear regression curve, PC = Pearson correlation coefficient.

survival upon auxin-induced BRCA1 depletion (Figure 1D). Importantly, complementation of the *EXO1*$^{-/-}$ cells with full-length *EXO1* cDNA, but not with the catalytic dead mutant D173A, rescued the toxicity of auxin-induced BRCA1 depletion (Figures S2C and S2D), indicating that the catalytic activity of EXO1 is essential for BRCA1-deficient cells. Moreover, re-expression of *BRCA1* in EXO1-depleted *BRCA1* knockout cells restored their viability (Figures S2E and S2F), validating that the synthetic lethality was due to on-target gene editing. Finally, we found that EXO1 is essential in the patient-derived *BRCA1*-mutated MDA-MB-436 cells[53,54] and in BRCA1-deficient (BRCA1 Δ exon 11) mouse embryonic fibroblasts (MEFs),[10] but not in their respective BRCA1-proficient control cells, showing that the synthetic lethal interaction is not cell type specific (Figures 1E, 1F, and S2G–S2J).

Similar to EXO1 loss, BLM deficiency significantly impaired clonogenic survival of auxin-treated *BRCA1-mAID* cells (Figures 1G and S2K). Interestingly, BLM depletion even further reduced clonogenic survival of BRCA1-depleted *EXO1*$^{-/-}$ cells (Figure 1G). These results indicate that BLM and EXO1 have unique, additive functions in promoting survival of BRCA1-deficient cells. Indeed, in an accompanying paper in this issue, Tsukada and Jones et al. show that BRCA1-deficient cells depend on BLM because of its role in resolving DNA replication intermediates,[55] which is unconnected to our proposed model below for EXO1. The rest of this study will therefore focus on EXO1.

BRCA1-mutated tumors exhibit elevated EXO1 expression

The dependency of BRCA1-deficient tumor cells on synthetic lethal interactors frequently manifests itself by high levels of expression or activity of the interactor, as has been shown for POLQ and PARP1.[31,56] We therefore investigated the correlation between *EXO1* expression levels and *BRCA1* mutation status in two previously published breast cancer cohorts.[1,57] Indeed, in both the pan-breast cancer cohort and the triple-negative breast cancer cohort, *EXO1* expression was elevated in *BRCA1*-mutated and *BRCA1* promoter-hypermethylated tumors compared with *BRCA1*-wild-type (WT) tumors (Figures 2A and S3A). The increased expression was comparable with the increase in *POLQ* expression. *MRE11* expression was not increased in BRCA1-deficient breast tumor samples, consistent with the lack of a synthetic lethal interaction with BRCA1 (Figures 2A and S3A).

To extrapolate the elevated *EXO1* expression found in *BRCA1*-mutated tumors to HR-deficient tumors in general, the TCGA breast cancer dataset was used to correlate genome-wide gene expression to HR deficiency (HRD) scores.[58] A strong positive correlation was observed between *EXO1* expression and HRD score, whereas such a correlation was absent for *MRE11* (Figure 2B). In fact, *EXO1* was among the top hits that showed the strongest positive correlation with the HRD score, with a Pearson correlation even higher than for *POLQ* (Figure 2C). The correlation between HRD score and *EXO1* expression was only marginally reduced when all *BRCA1*-mutant samples were removed from the analysis (Figure S3B). Thus, elevated *EXO1* expression in HR-deficient tumors is not solely driven by *BRCA1* mutations, implying that other HR-deficient cells might also depend on EXO1 function.

EXO1 loss is essential for BARD1-deficient cells, but not BRCA2-deficient cells

To explore which other causes of HR deficiency result in dependency on EXO1 activity, we started with the analysis of BARD1-deficient cells. BARD1 forms an obligatory heterodimer with BRCA1, and both proteins stabilize each other; hence, BARD1 is functionally closely related to BRCA1.[52,59,60] This functional relationship is reflected in the observation that also hereditary *BARD1*-mutations predispose carriers to breast cancer tumors, although the occurrence and cancer risk is lower than that for *BRCA1*-mutations.[61] To study the synthetic lethal interaction between BARD1 and EXO1, we depleted EXO1 in a previously described HCT116 cell model with endogenously AID-tagged

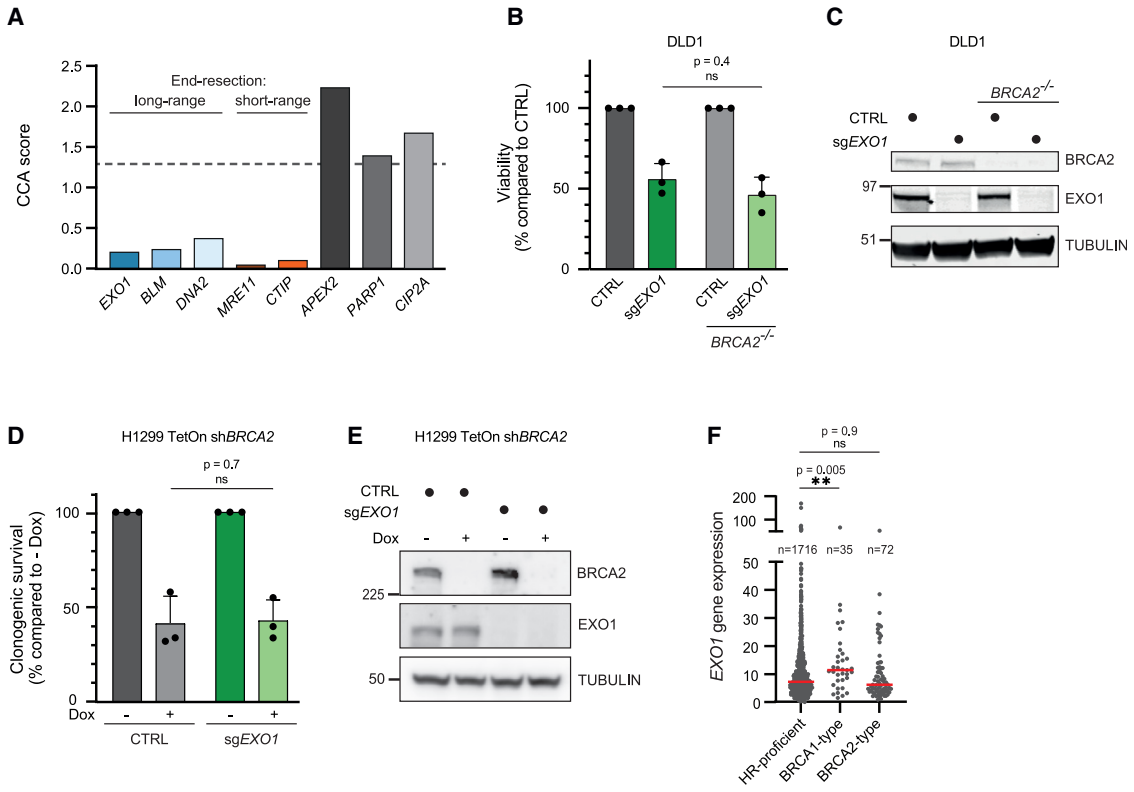

Figure 3. EXO1 loss is not lethal in BRCA2-deficient cells

(A) A published gene essentiality screen in BRCA2-proficient and -deficient DLD1 cells[41] was mined to extract the CCA scores for the indicated genes. A higher CCA score indicates a unique essentiality in BRCA2-deficient cells compared with proficient cells. Dashed line indicates the cut-off for a significant CCA score (based on Adam et al.[41]).

(B) DLD1 WT and *BRCA2*$^{-/-}$ cells were infected with empty vector (CTRL) or EXO1-targeting sgRNA and viability was measured using CellTiter-Glo (n = 3, mean + SD, ns = p > 0.05, paired t test).

(C) Lysates of the indicated DLD1 cells indicated in (B) analyzed by western blotting.

(D) H1299 cells carrying a doxycycline-inducible BRCA2 shRNA were transduced with an *AAVS1*-targeting (CTRL) or *EXO1*-targeting sgRNA, followed by a clonogenic survival assay in the absence or presence of 10 μg/mL doxycycline (n = 3, mean + SD, ns = p > 0.05, paired t test).

(E) Western blot analysis of the lysates of the H1299 TetOn shBRCA2 cells studied in (D).

(F) CHORD analysis[3] was applied to determine the HR-status of tumors of a pan cancer dataset (n = 1,823) and *EXO1* expression was plotted (red line indicates median, ns = p > 0.05, **p < 0.01, Kruskal-Wallis with Dunn's multiple comparisons test).

BARD1.[62] As expected by the functional connection between BRCA1 and BARD1, BARD1-depleted cells, but not the control cells, showed reduced viability upon EXO1-depletion (Figures S3C and S3D). These data indicate that EXO1 dependency extends beyond *BRCA1*-mutated tumors.

Next, we explored whether BRCA2 deficiency resulted in a dependency on EXO1 activity. For this, we again mined the results of the CRISPR gene essentiality screens from Adam et al. which also included BRCA2-deficient cells.[41] Surprisingly, no synthetic lethal interaction was observed between BRCA2 deficiency and EXO1 loss (Figure 3A). This is consistent with another recently published CRISPR screen in BRCA2-depleted HEK293A cells that also failed to identify a dependency on *EXO1* expression.[63] To validate these results, we depleted EXO1 in WT or *BRCA2*$^{-/-}$ DLD1 cells using CRISPR-Cas9. In line with the results of the CRISPR essentiality screens, the viability of BRCA2/EXO1 double-depleted cells was similar to the viability of EXO1-depleted cells (Figures 3B and 3C). As a second approach, we depleted EXO1 in H1299 cells containing doxycycline (dox)-inducible *BRCA2* shRNA.[64] Similarly to what we observed in DLD1 cells, EXO1 loss did not affect the clonogenic survival of BRCA2-depleted cells compared with control cells (Figures 3D and 3E), confirming that BRCA2-deficient cells do not depend on EXO1 for survival.

Based on these data, we expected that *BRCA2*-mutated tumors do not show increased *EXO1* expression. Because the two cohorts described above did not contain sufficient *BRCA2*-mutated tumors to draw strong conclusions, we included a third pan-cancer cohort that was divided into HR-proficient, BRCA1-type HR-deficient (n = 35), or BRCA2-type HR-deficient subgroups (n = 72), based on the analysis of genome-wide mutational footprints (PCAWG and Hartwig Medical Foundation datasets[3,65]). Indeed, we did not observe the upregulation of *EXO1* in BRCA2-type tumors, whereas BRCA1-type tumors showed elevated *EXO1* expression (Figure 3F). These results suggest that also in tumors, EXO1 is essential for BRCA1-, but not BRCA2-deficient cells.

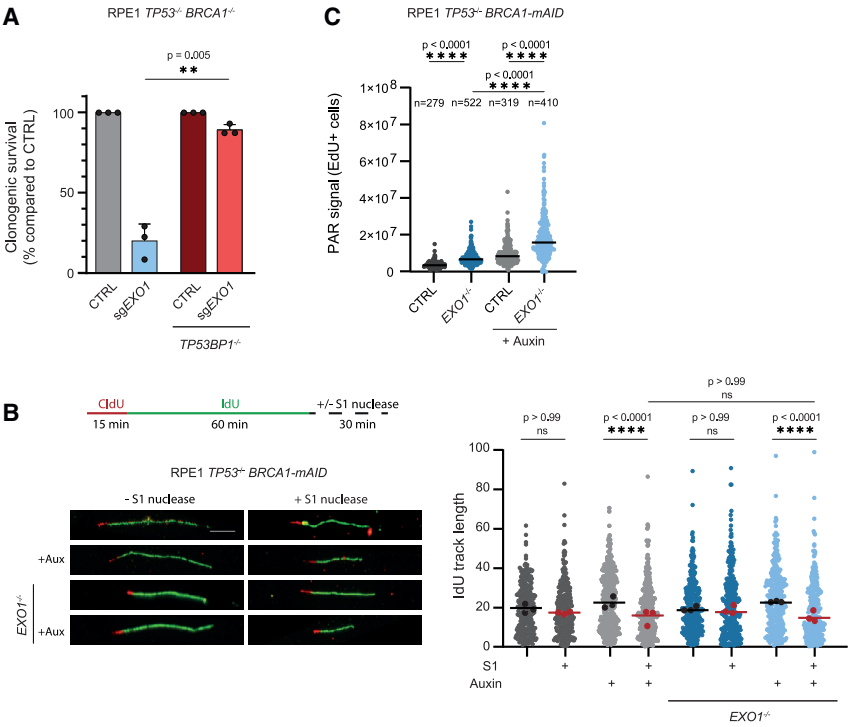

Figure 4. EXO1 depletion causes increased S phase PARylation

(A) RPE1 hTERT *TP53*$^{-/-}$ *BRCA1*$^{-/-}$ cells expressing Cas9, either *TP53BP1*$^{+/+}$ or *TP53BP1*$^{-/-}$, were transduced with an *AAVS1*-targeting (CTRL) or *EXO1*-targeting sgRNA, followed by a clonogenic survival assay (n = 3, mean + SD, **p < 0.01, paired t test). Western blot of lysates shown in Figure S4A.

(B) Analysis of replication fiber length after incubation with and without S1 nuclease. Left panel shows setup of experiment (top) and images of representative fibers (bottom), right panel shows quantification (n = 3, at least 100 fibers were analyzed per condition, per replicate; black or red dots indicate median per experiment and the line indicates their average, ns = p > 0.05, ****p < 0.0001, Kruskal-Wallis followed by Dunn's multiple comparison test).

(C) Indicated RPE1 cell lines were incubated with EdU and PARGi, followed by IF microscopy to quantify PAR levels. A representative of two independent experiments is shown, black line indicates median (****p < 0.0001, Mann Whitney).

Cells deficient for EXO1 and BRCA1 accumulate replication-associated lesions

Both BRCA1 and EXO1 play critical roles in genome maintenance with described functions during DSB repair and Okazaki fragment maturation.[39,59,66] Moreover, BRCA1 plays a role in replication fork stability and EXO1 in mismatch repair (MMR).[59,66,67] We aimed to pinpoint which of these processes causes lethal toxicity when disrupted by loss of BRCA1 and EXO1. First, we assessed cell viability in *BRCA1*$^{-/-}$ cells in which 53BP1 was inactivated because its loss restores HR[68,69] and prevents ssDNA gap formation in *BRCA1*$^{-/-}$ cells[38,39] without rescuing replication fork destabilization.[70] Loss of 53BP1 fully restored clonogenic survival of EXO1-depleted *BRCA1*$^{-/-}$ cells (Figures 4A and S4A). Hence, these experiments ruled out that destabilized replication forks in BRCA1-deficient cells generate a dependency on EXO1.

To explore whether defective MMR caused the lethality of EXO1 loss in BRCA1-deficient cells, we checked the essentiality of other core MMR factors (MLH1, MSH2, MSH3, MSH6, PMS1, and PMS2) in the aforementioned CRISPR screen.[41] Depletion of none of these MMR factors reduced viability of BRCA1-proficient cells nor did it result in synthetic lethality with BRCA1 loss (Figure S4B), thus arguing against the function of EXO1 in MMR being required for the survival of BRCA1-deficient cells.

Next, we evaluated whether BRCA1 and EXO1 loss affected ssDNA gap formation, given the strong association between ssDNA gaps and genome instability in BRCA-deficient cells.[39,40,71] For this, we pulsed cells with 5-chloro-2′-deoxyuridine (CldU) and 5-iodo-2′-deoxyuridine (IdU) and quantified replication tract length using DNA fiber analysis before and after incubation with the ssDNA-specific S1 nuclease.[72] Confirming previous observations, we found that BRCA1 depletion caused an increase in ssDNA gaps.[39,40,71] In contrast, EXO1 depletion did not affect ssDNA levels of either WT control or BRCA1-deficient cells (Figure 4B). As an alternative readout for the presence of ssDNA, we assessed CHK1 phosphorylation which occurs downstream of ssDNA-induced ATR activation.[73] Although BRCA1-depletion increased CHK1 phosphorylation, consistent with the presence of ssDNA, this was not further increased by EXO1 loss (Figure S4C).

Finally, we measured S phase poly(ADP-ribosyl)ation (PARylation), which has been reported to reflect the presence of ssDNA gaps and more particularly unprocessed Okazaki fragments,[74,75] although it is also induced at DSBs and other lesions.[76] We observed increased PARylation in our BRCA1-deficient cell lines (Figures 4C and S4D), which was specific to S phase cells. These data are consistent with the model proposed by the Cantor lab that accumulation of unprocessed Okazaki fragments underlies the formation of ssDNA gaps in BRCA1-deficient cells.[39] Remarkably, we also observed increased levels of S phase PARylation colocalizing with nascent 5-ethynyl-2'-deoxyuridine (EdU)-labeled DNA upon EXO1 depletion (Figures 4C, S4D, and S4E), suggesting that human cells deficient for EXO1 accumulate unprocessed Okazaki fragments, similar to what has been found in yeast and *C. elegans* cells.[29,77,78] Moreover, we detect an additive effect on S phase PARylation when EXO1 was depleted in BRCA1-deficient cells (Figures 4C and S4D), suggesting that loss of both factors results in an even higher accumulation of unprocessed Okazaki fragments than in either single mutant. Of note, this EXO1 loss-induced phenotype is consistent with previous findings in FEN1-deficient cells, in which accumulation of unprocessed Okazaki fragments is detected by increased PARylation but not by S1 nuclease-based DNA fiber assays.[39,79,80]

Interestingly, EXO1 loss induced a similar increase in S phase PAR levels in BRCA2-deficient cells as in BRCA1-deficient cells (Figure S4F). Hence, these data suggest that the accumulation of

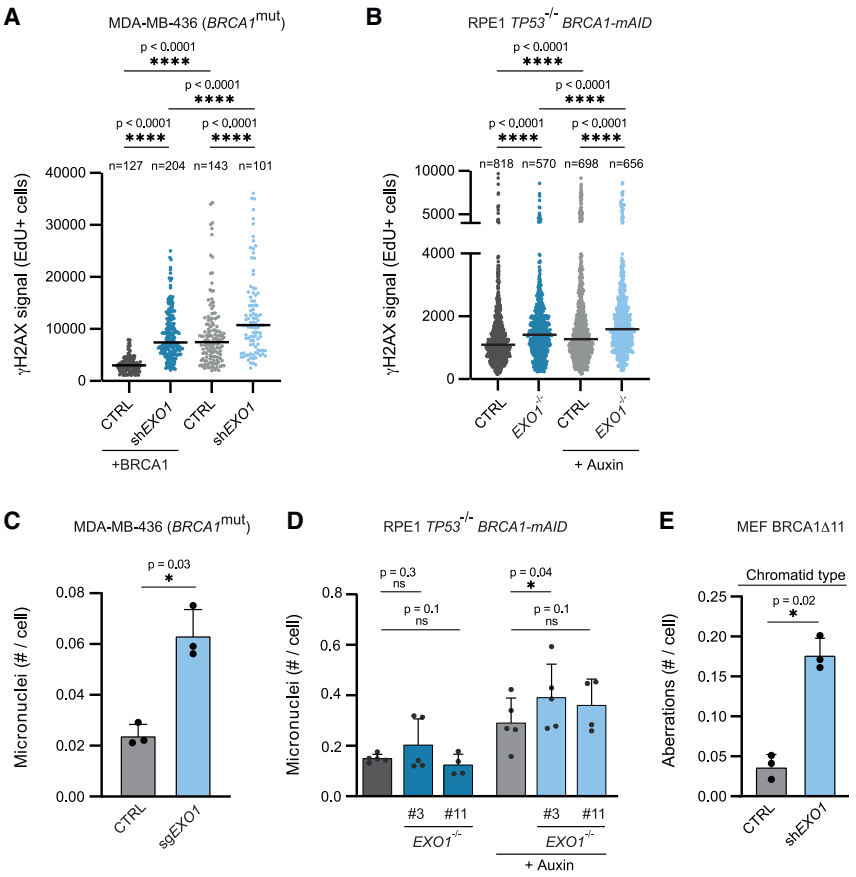

Figure 5. Genomic instability in BRCA1-deficient cells is exacerbated by EXO1 depletion

(A) Nuclear γH2AX intensity in S phase (EdU+) cells was analyzed by IF microscopy in *BRCA1*-mutated MDA-MB-436 cells (+BRCA1-reconstituted with BRCA1 cDNA). A representative of two independent experiments is shown, black line indicates median (****p < 0.0001, Mann Whitney).

(B) RPE1 hTERT *TP53*$^{-/-}$ BRCA1-mAID-GFP cells, either *EXO1*$^{+/+}$ or *EXO1*$^{-/-}$, were treated with 500 μM auxin for 48 h to deplete BRCA1 or left untreated. Nuclear γH2AX intensity in S phase (EdU+) cells was analyzed by automated IF microscopy imaging. A representative of two independent experiments is shown, black line indicates median (****p < 0.0001, Mann Whitney). Figure S5A shows representative microscopy images.

(C) *BRCA1*-mutated MDA-MB-436 cells were infected with empty vector (CTRL) or *EXO1*-targeting sgRNA. This was followed by DAPI staining and microscopic quantification of the number of micronuclei (n = 3, mean + SD, *p < 0.05, ratio paired t test).

(D) RPE1 hTERT *TP53*$^{-/-}$ BRCA1-mAID-GFP cells, either *EXO1*$^{+/+}$ or *EXO1*$^{-/-}$, were treated with 500 μM auxin for 48 h to deplete BRCA1 or left untreated. This was followed by Hoechst staining and microscopic quantification of the number of micronuclei (n = 5, mean + SD, ns = p > 0.05, *p < 0.05, ratio paired t test).

(E) MEFs with a homozygous exon 11 deletion in the *BRCA1* gene (Δ11) were infected with control or *EXO1*-targeting shRNA, followed by metaphase spread analysis (n = 3, >40 metaphases per replicate, mean + SD, *p < 0.05, ratio paired t test).

unprocessed Okazaki fragments cannot be the sole cause of the lethality of EXO1 loss in BRCA1-deficient cells. Rather, we postulate that the unprocessed Okazaki fragments cause a downstream lesion—most likely a DSB—that may be more toxic in a BRCA1-deficient background than a BRCA2-deficient background. We therefore continued to investigate the contribution of defective DSB repair to the toxicity of EXO1 loss in BRCA1-deficient cells.

Genomic instability in BRCA1-deficient cells is exacerbated by EXO1 depletion

To study whether unresolved DSBs are involved in the synthetic lethal interaction between BRCA1 deficiency and EXO1 loss, we analyzed γH2AX levels as a marker for unresolved DSBs in the different genomic backgrounds under unperturbed growth conditions using quantitative imaging-based cytometry (QIBC). In both MDA-MB-436 and RPE1 cells, BRCA1 deficiency or EXO1 loss increased γH2AX levels in S phase cells (Figures 5A, 5B, and S5A). Importantly, depleting both EXO1 and BRCA1 further increased γH2AX levels (Figures 5A, 5B, and S5A), indicating that these cells suffer from high levels of unrepaired DSBs. In contrast, BRCA2-deficient DLD1 cells, which tolerate loss of EXO1, did not show any increase in γH2AX levels upon depletion of EXO1 (Figures S5B and S5C).

Next, we studied the spontaneous formation of micronuclei and chromosomal aberrations in our different cell models, as these are a direct consequence of aberrant DSB repair.[81,82] EXO1 loss induced micronuclei formation in *BRCA1*-mutant MDA-MB-436 cells and in BRCA1-depleted RPE1 *BRCA1*-mAID cells (Figures 5C and 5D). Notably, this phenotype was specific for BRCA1-deficient cells as neither BRCA1-proficient cells (Figure 5D) nor BRCA2-deficient DLD1 cells showed an increase in micronuclei formation upon EXO1 depletion (Figure S5D).

Additionally, double depletion of BRCA1 and EXO1 caused increased chromosomal aberrations compared with cells depleted for either factor alone. This was predominantly caused by a substantial increase in chromatid aberrations (chromatid breaks and radials) upon EXO1 depletion, as observed both in BRCA1-depleted RPE1 cells and in *BRCA1*-mutated MEFs (Figures 5E, S5E, and S5F). Together, these data indicate that the combined loss of BRCA1 and EXO1 results in an accumulation of DSBs and consequently in genomic instability. Our findings support a model where the absence of EXO1, in conjunction with the lack of BRCA-dependent HR, results in a defect to resolve DSBs through an alternative repair pathway. This alternative pathway appears to remain operational in BRCA2-deficient cells but is compromised in BRCA1-deficient cells.

The toxicity of EXO1 loss is caused by impaired DSB repair via SSA in BRCA1-deficient cells, but not in BRCA2-deficient cells

To examine a possible additional DSB repair defect on top of HR loss in cells lacking both BRCA1 and EXO1, we directed our

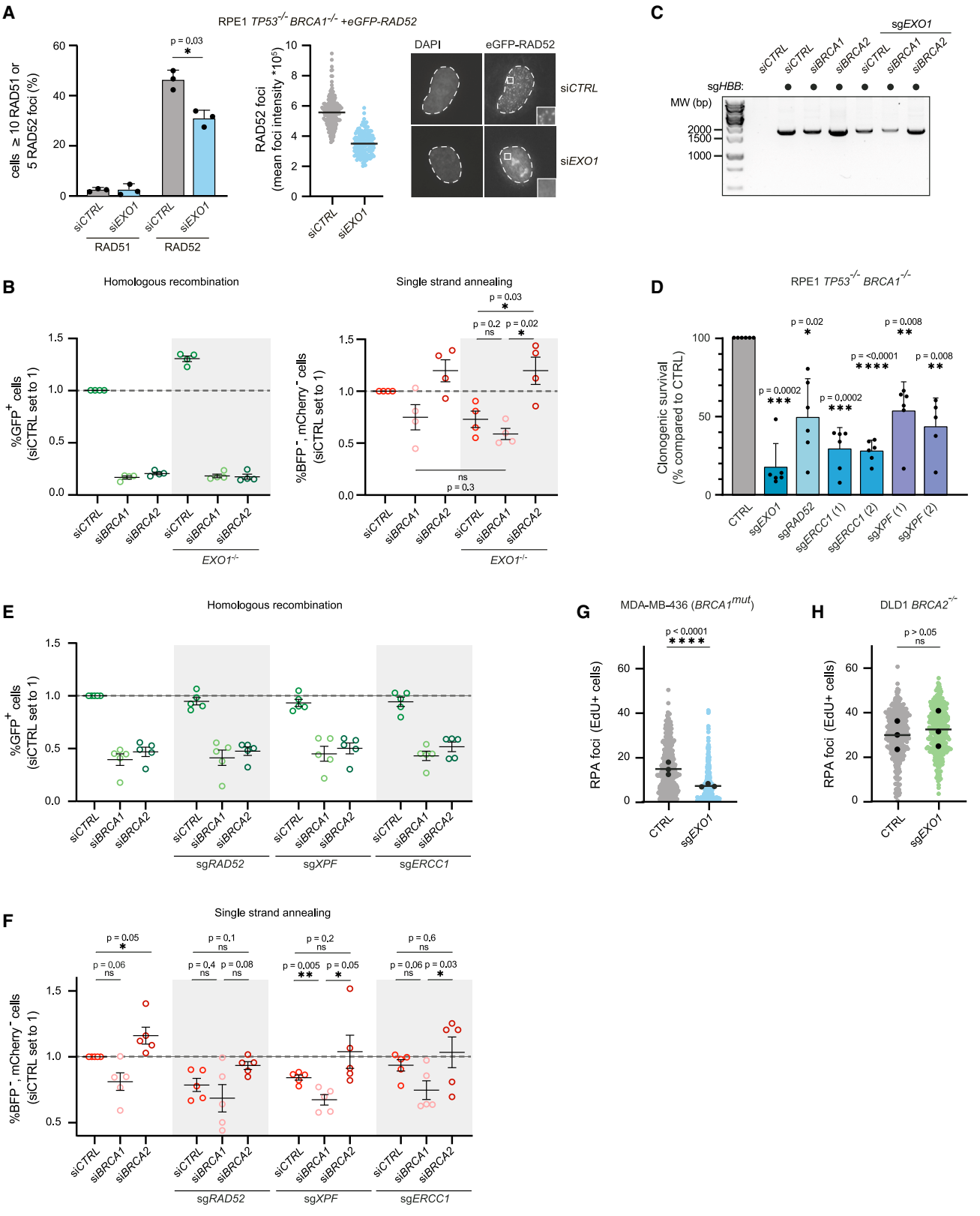

(legend on next page)

attention to SSA, which is dependent on long-range end resection and hence is promoted by EXO1.[23,83,84] We therefore hypothesized that cells depleted for both BRCA1 and EXO1 suffer from a combined deficiency in HR and SSA. To study this, we assessed ionizing irradiation-induced foci (IRIF) of RAD51 and RAD52 in the different genetic backgrounds as a readout of HR and SSA, respectively. As expected, RAD51 IRIF were strongly reduced in BRCA1- and BRCA2-deficient cells, and depletion of EXO1 did not further abrogate this (Figures 6A, S6A, S6C, and S6E). In contrast, RAD52 IRIF were significantly reduced by EXO1 depletion in BRCA1-deficient cells, both in number and intensity. In contrast, EXO1 loss did not affect RAD52 foci in BRCA2-deficient cells (Figures 6A, S6A, S6B, S6D, and S6E). In fact, BRCA2-deficient cells showed elevated RAD52 IRIF compared with control cells, regardless of the EXO1 status, in line with earlier studies showing an increase in SSA upon BRCA2 loss (Figure S6D).[85–87]

As a second readout of HR and SSA, we made use of our DSB-Spectrum_V3 reporter, in which the frequency of HR and SSA repair of a Cas9-induced DSB can be monitored by flow cytometry (Figure S6F).[23] As expected, depletion of BRCA1 or BRCA2 resulted in strong inhibition of HR (Figures 6B and S6G). In contrast, BRCA2 depletion increased SSA levels, consistent with our RAD52 foci analysis. BRCA1 depletion resulted in lower levels of SSA, in line with published results.[85,88,89] *EXO1*$^{-/-}$ cells had reduced SSA and increased HR compared with control cells, both consistent with previous work.[23] Interestingly, loss of EXO1 further decreased SSA levels in BRCA1-depleted cells, albeit not significant, whereas it did not affect the elevated SSA in BRCA2-depleted cells (Figure 6B). Consequently, the reporter experiments confirm the results obtained by RAD51 and RAD52 foci analysis and show that BRCA1/EXO1-depleted cells have a combined HR and SSA defect, whereas the BRCA2/EXO1-depleted cells retain SSA activity.

Of note, neither EXO1 nor BRCA1 depletion substantially affected mutagenic end-joining, which can be monitored simultaneously with HR and SSA in DSB-Spectrum_V3 cells (Figure S6H), arguing against excessive end-joining inducing the cellular toxicity. A similar result was obtained using DSB-Spectrum_V1, a different variant of our reporter that is designed to quantify error-free classical non-homologous end-joining (cNHEJ), rather than the collective mutagenic end-joining measured by DSB-Spectrum_V3[23] (Figure S6I). A possible caveat of these DSB-reporter assays is the lack of a positive control that results in a strong upregulation of end-joining, although we have previously shown that inhibiting HR results in a small increase of end-joining,[23] resembling our data on BRCA1-depletion, but not EXO1-depletion in Figure S6I. In addition, the frequency of end-joining was similar in BRCA1- and BRCA2-depleted *EXO1*-deficient cells in both reporter assays (Figures S6H and S6I). Together, these results indicate that the synthetic lethality between EXO1 loss and BRCA1 deficiency is not caused by excessive end-joining activity, but rather by decreased SSA.

Finally, we examined SSA repair of a Cas9-induced DSB at the *HBB* locus, which is prone to SSA due to the presence of the highly homologous adjacent *HBD* gene (Figure S6J).[23] For this, HEK293T cells were transfected with a Cas9 cDNA and an *HBB*-targeting sgRNA, followed by PCR analysis of the target site using primers designed to amplify the SSA repair product. Consistent with our other findings, SSA levels were decreased by individual depletion of EXO1 or BRCA1 with an additive effect on BRCA1/EXO1 double-depleted cells (Figure 6C). Moreover, considerably less SSA repair product was retrieved from BRCA1/EXO1 double-depleted cells than from BRCA2/EXO1-depleted cells. Altogether, our three independent assays for SSA indicate that cells deficient for both BRCA1 and EXO1 have a severely reduced capacity to repair DSBs due to a dual defect in both HR and SSA, whereas BRCA2-deficient cells retain high SSA activity even upon EXO1 loss.

End resection and SSA are essential for survival in BRCA1-deficient cells

To further study the importance of SSA in HR-deficient cells, we tested the essentiality of SSA factors other than EXO1. SSA remains a poorly described pathway and all described SSA factors, including RAD52, and ERCC1-XPF also function in other genome maintenance pathways.[90] Nevertheless, we assessed survival of BRCA1-deficient RPE1 cells and BRCA2-deficient DLD1 cells upon depletion of those SSA factors. Similar to the loss of EXO1, loss of RAD52, XPF, or ERCC1 also reduced the viability of *BRCA1*$^{-/-}$ cells (Figures 6D and S7A). Interestingly,

Figure 6. Survival of BRCA1-deficient cells is dependent on the function of EXO1 in SSA

(A) Indicated RPE1 cells expressing eGFP-RAD52 were transfected with a control (siCTRL) or *EXO1*-targeting siRNA, exposed to IR (10 Gy) and analyzed by IF microscopy for RAD51 and RAD52 foci formation 3 h post-IR. Left panel shows foci quantification (n = 3, mean + SD, *p < 0.05, paired t test), middle panel shows the mean eGPP-RAD52 foci intensity (a representative of three independent experiments is shown, black lines indicate mean) and right panel shows representative microscopy images of eGFP-RAD52 foci. Western blot of lysates shown in Figure S6A.

(B) HEK293T cells carrying the DSB-Spectrum_V3 reporter, either WT or *EXO1*$^{-/-}$, were transfected with a control (siCTRL), *BRCA1*- or *BRCA2*-targeting siRNA, followed by a second round of transfection with a Cas9 cDNA and sgRNA targeting the reporter locus. Next, cells were analyzed by flow cytometry to quantify repair by the indicated pathways (n = 4, mean ± SEM, ns = p > 0.05, *p < 0.05, ratio paired t test). Western blot of lysates shown in Figure S6G.

(C) HEK293T DSB-Spectrum_V3 cells, either WT control (sg*AAVS1*) or depleted for EXO1 (sg*EXO1*) were transfected with indicated siRNAs. Next, cells were transfected with Cas9 cDNA and an *HBB*-targeting sgRNA. The SSA repair product was PCR-amplified and analyzed by agarose gel electrophoresis. Representative agarose gel of three replicates.

(D) Clonogenic survival assay of Cas9-expressing RPE1 hTERT *TP53*$^{-/-}$ *BRCA1*$^{-/-}$ cells that were transduced to express the indicated sgRNAs (n = 6, mean + SD, *p < 0.05, **p < 0.01, ***p < 0.001, ****p < 0.0001, one-way ANOVA, post hoc Dunnett's, compared with CTRL). Western blot of lysates shown in Figure S7A.

(E and F) As in (B), but now for DSB-Spectrum_V3 reporter cells depleted for RAD52, XPF, or ERCC1 (HR: E, SSA: F) (n = 5, mean ± SEM, ns = p > 0.05, *p < 0.05, **p < 0.01, ratio paired t test). Western blot of lysates shown in Figure S7D.

(G and H) RPA foci in S phase (EdU+) cells were analyzed by IF microscopy in *BRCA1*-mutated MDA-MB-436 cells (G) or DLD1 *BRCA2*$^{-/-}$ cells (H) infected with empty vector (CTRL) or *EXO1*-targeting sgRNA 3 h post-5 Gy IR (n = 3, mean, ns = p > 0.05, ****p < 0.0001, Mann Whitney). RPA foci formation in BRCA1-complemented MDA-MB-436 control samples is shown in Figure S7F.

viability of BRCA2-deficient cells was only modestly (RAD52) or not at all (XPF/ERCC1) affected by loss of these factors (Figures S7B and S7C). To correlate these viability effects to SSA efficacy, we depleted RAD52, XPF, or ERCC1 in DSB-Spectrum_V3 reporter cells in combination with siRNA-mediated BRCA1 or BRCA2 depletion. We observed similar results for all tested SSA factors: although depletion of these factors did not affect HR, combined loss of BRCA1 with either RAD52, XPF, or ERCC1 resulted in the lowest frequency of SSA compared with loss of these factors alone or with loss of these factors in combination with BRCA2 (Figures 6E, 6F, and S7D). Although individual differences did not always reach statistical significance, the collective data indicate that BRCA1-deficient cells are more susceptible to disruption of SSA than BRCA2-deficient cells, which is most likely attributed to the already impaired SSA by loss of BRCA1 alone. Moreover, our results show a strong correlation between SSA activity and survival of HR-deficient cells, suggesting that SSA functions as an essential backup for DSB repair.

The toxicity of RAD52 loss has been ascribed to functions for RAD52 in promoting both SSA and residual HR in BRCA1-deficient cells.[32,33] Since we could detect some residual RAD51 IRIF in our BRCA1-deficient cells, we asked whether RAD52, or other SSA factors, would be required for this residual HR. Analysis of RAD51 IRIF showed that the residual HR in these cells was not reduced by RAD52 depletion nor by depletion of EXO1, XPF, or ERCC1 (Figure S7E). Of note, also in our DSB-Spectrum_V3 reporter assays, RAD52-depletion did not further decrease HR frequency in cells depleted for either BRCA1 or BRCA2 using siRNAs (Figure 6E). This indicates that the loss of EXO1 or any of the other SSA factors does not cause lethality in BRCA1-deficient cells by affecting residual HR levels.

To elucidate why BRCA2-deficient cells can perform SSA in the absence of EXO1, we examined the role of EXO1 in end resection in both BRCA-deficient settings. BRCA1-depleted cells showed reduced resection upon EXO1 depletion in both MDA-MB-436 cells and RPE1 cells (Figures 6G, S7G, and S7H). In contrast, BRCA2-deficient cells consistently retained higher resection levels upon EXO1 depletion than BRCA1-deficient cells. In DLD1 BRCA2-deficient cells, resection was not affected at all by EXO1 loss (Figure 6H), whereas in our siRNA-mediated depletions in RPE1 cells, EXO1-depletion did reduce resection in BRCA2-deficient cells, but these levels remained higher than in the BRCA1/EXO1-depleted setting (Figures S7G and S7H). In WT control cells, the end resection phenotype upon EXO1 depletion is cell line-dependent (Figures S7F and S7G), consistent with the published literature showing differences in redundancy with DNA2-mediated end resection between cell lines.[10,20,91] Altogether, these data suggest that BRCA1-deficient cells highly depend on EXO1 for long-range end resection, whereas BRCA2-deficient cells show sufficient levels of EXO1-independent long-range end resection to perform SSA.

BRCA1-mutated tumors show increased usage of SSA

Our data are consistent with a model in which EXO1 loss leads to unresolved DSBs in BRCA1-deficient cells because of an enhanced damage load in combination with insufficient SSA and HR activity. In contrast, BRCA2/EXO1-deficient cells retain SSA activity to resolve the DSBs, allowing survival (Figure 7A). Culminating from this model, *BRCA1*-mutated tumors are expected to repair DSBs by EXO1-mediated SSA more frequently than HR-proficient tumors. To further explore this hypothesis, we searched for signatures of SSA usage in genomes of the pan-cancer cohort we used in Figure 3F. We defined deletions flanked by homologous sequences of more than 10 base pairs (bps) as genetic "scars" indicative of DSB repair by SSA. This broad definition will include the majority of SSA repair events while excluding most POLQ-mediated alt-EJ that generally occurs between smaller-sized homology regions.[27] In line with our model, the number of genetic SSA scars was higher in BRCA1-type HR-deficient tumor samples than in HR-proficient tumor samples (Figure 7B). BRCA2-type tumors carried an even higher load of SSA scars than BRCA1-type tumors (Figure 7B), fully consistent with higher levels of SSA in BRCA2-deficient cells relative to BRCA1-deficient cells (Figure 6B). Similar results were obtained when using a more stringent SSA scar definition containing a homology requirement of more than 50 bp (Figure S7I). Recent data using linked-read whole genome sequencing identified increased SSA usage as a discriminating feature of BRCA2-deficient tumors,[92] which is fully consistent with our data. Importantly, the increased SSA usage of tumors correlated with higher *EXO1* expression (Figure 7C). Hence, these data indicate that in tumors, BRCA1 deficiency induces compensatory DSB repair by EXO1-mediated SSA.

DISCUSSION

Here, we demonstrate that genetic depletion of EXO1 is severely toxic to BRCA1-deficient cells, identifying a potential novel target for future therapy development. EXO1 loss in BRCA1-deficient cells increases chromosomal instability that is accompanied by replication-dependent DSB accumulation. Our data suggest that these DSBs are left unrepaired due to a dual incapacity to perform HR and SSA (Figure 7A). These *in vitro* data are substantiated by analyses of tumor samples, which indicated that *BRCA1*-mutated tumors show elevated *EXO1* expression and bear increased numbers of SSA-derived genetic scars, suggesting the compensatory upregulation of SSA in the absence of HR.

Unexpectedly, we found that in BRCA2-deficient cells loss of EXO1 affects neither DSB accumulation nor chromosomal stability. Hence, these cells tolerate EXO1 loss. Since both BRCA1 and BRCA2 loss results in HR deficiency, an HR defect by itself cannot explain why BRCA1-deficient cells depend on EXO1 for survival. Our data indicate that BRCA1 loss reduces SSA, whereas BRCA2 loss promotes SSA, consistent with published data.[85,87–89] SSA might be promoted in BRCA2-deficient cells by enhanced RAD52 recruitment to resected ends due to defective RAD51 loading. Consistently, SSA was shown to be promoted by loss of PALB2 or by expression of a BRCA1 mutant with defective RAD51 loading capacity due to a mutation in its PALB2-binding domain.[88] Unlike BRCA2, BRCA1 also functions in end resection, which is likely to explain its SSA-promoting function.[85,86,93] Our data furthermore strongly suggest that EXO1 promotes SSA in BRCA1-deficient cells but is dispensable for this process in BRCA2-deficient cells. This correlates with a strong dependency on BRCA1-deficient cells, but not

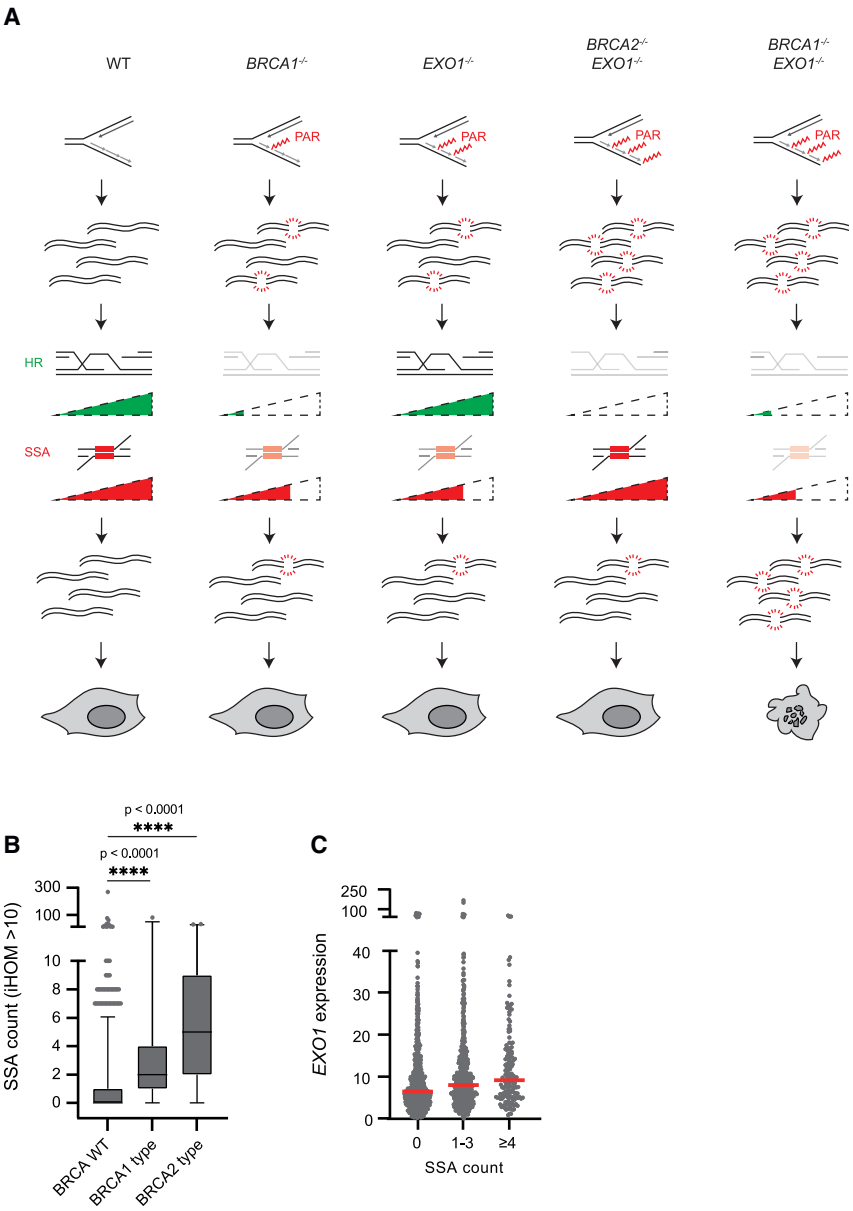

Figure 7. BRCA1-deficient tumors have more SSA scars than BRCA1-proficient tumors

(A) Model of the mechanism causing synthetic lethality between BRCA1-deficiency and EXO1 loss. Levels of transparency indicate levels of pathway activity.

(B) Whole genome sequencing data of pan cancer tumor samples[65] was analyzed to quantify the number of genetic scars indicative of DSB repair by SSA, here defined as deletions flanked by homologous sequences of >10 bp. CHORD analysis was used to determine HR-status[3] (****p < 0.0001, Kruskal-Wallis with Dunn's multiple comparisons test).

(C) Tumor samples from a pan-cancer cohort were binned based on SSA scar count, and the *EXO1* expression was plotted for each tumor sample.

BRCA2-deficient cells on EXO1 for end resection. This dependency of BRCA1-deficient cells on EXO1-mediated resection might correspond to a previously described defect of these cells to recruit DNA2, the second nuclease involved in long-range end resection.[94]

Upon induction of replication stress in BRCA-deficient cells, for example by treatment with hydroxyurea, EXO1 has been described to extend ssDNA gaps and degrade reversed forks.[66,95–97] Under these conditions, EXO1 activity promotes genomic instability in BRCA-deficient cells. Although this negative effect might be resolved upon EXO1 depletion, our data suggest that other problems emerge following EXO1 loss in unperturbed conditions. We found that loss of EXO1 strongly increased S phase PAR levels in WT and BRCA1- and BRCA2-depleted backgrounds. Research by the Caldecott lab has shown that unprocessed Okazaki fragments are the main source of S phase PAR levels in normal cycling cells.[79] Our data would thus suggest that EXO1 functions in Okazaki fragment processing in human cells, consistent with findings in *C. elegans* and *S. cerevisiae*.[29,77,78] In this scenario, it is likely the flap-endonuclease activity of EXO1 that is involved in Okazaki fragment metabolism.[98,99] Notably, the toxicity of PARP inhibition has recently been attributed to unligated Okazaki fragments,[80] and loss of FEN1, the primary endonuclease in Okazaki fragment processing, is also synthetically lethal with BRCA deficiency.[100] Hence, defective Okazaki fragment maturation is a prime vulnerability of BRCA-deficient cells. EXO1 is unique in this context because it is only essential to BRCA1-deficient cells, whereas PARP inhibition and FEN1 loss also kill BRCA2-deficient cells.[43,44,100] This might be explained by a stronger increase in unprocessed Okazaki fragments by FEN1 and PARP1 loss compared with EXO1 loss, as these two proteins are more essential for this process.[101] Alternatively, unlike loss of EXO1, loss of FEN1 or PARP inhibition also impairs alt-EJ,[100,102–104] which might exacerbate the toxic effects of unligated Okazaki fragments in both BRCA-deficient contexts.

In line with this, it seems unlikely that unprocessed Okazaki fragments are the sole cause for the lethality since we observed high PAR levels in both BRCA1- and BRCA2-deficient cells. Alternatively, it is conceivable that accumulation of such lesions in an HR-deficient background may boost the need for an alternative DSB repair pathway since unprocessed Okazaki fragments or other ssDNA nicks/gaps can be converted into DSBs when encountered by replication forks, for example, upon PARP inhibition.[95,105–108] Indeed, impaired SSA can explain the unique sensitivity of BRCA1-deficient, but not BRCA2-deficient cells to EXO1 loss. All in all, our data suggest a model where

EXO1 loss results in double trouble for BRCA1-deficient cells by both increasing the DSB load and impairing the resolution of these breaks (Figure 7A).

EXO1 loss was generally well tolerated in all our BRCA1-proficient cell models, in line with collective results of gene essentiality screens in 1,162 different cell lines.[109] This suggests that there is a window of opportunity for selective killing of BRCA1-deficient tumor cells by targeting of EXO1. However, we do note that EXO1 loss induces some DNA stress also in a BRCA1-proficient setting, as indicated by increased PARylation and γH2AX levels. This notion should be taken along during the development of EXO1-targeting therapeutics, and side effects should be carefully monitored.

Similar to SSA, POLQ-mediated alt-EJ is essential in BRCA-deficient cells.[28,31] This suggests that these pathways are not simply redundant but complement each other to repair DSBs that remain unresolved due to HR deficiency. Indeed, previous research has shown that each pathway repairs a unique set of DSBs.[27] Furthermore, POLQ has a specific function in DSB repair during mitosis.[110–113] We believe this provides an opportunity to target both pathways simultaneously to improve tumor eradication and reduce the risk of resistance to either therapy individually. In conclusion, we show that EXO1 is essential for BRCA1-deficient cells, but not BRCA2-deficient cells. Therefore, EXO1 is a promising novel target for the treatment of BRCA1-deficient tumors, and the development of inhibitors directed at its nuclease activity should therefore be considered for use in monotherapy or combination therapy.

Limitations of the study

In this study, we have identified and characterized a dependency on EXO1 activity as a unique vulnerability of BRCA1-deficient cells. We were able to confirm this dependency in a variety of BRCA1- and BARD1-deficient human and mouse cell models, but the studies were restricted to cell lines. To validate if the synthetic lethal interaction between EXO1 and BRCA1 can be extrapolated from cell lines to more clinically relevant models, future research should be directed at studying this interaction in organoids and mouse tumor models. Such studies are also essential to monitor potential side effects of EXO1 depletion that might occur on the organismal level but are missed when studying cells in culture. Furthermore, we show that the catalytic activity of EXO1 is required for the viability of BRCA1-deficient cells, highlighting the therapeutic potential of targeting its catalytic activity with small molecule inhibitors. However, all our studies were done using genetic depletion and reconstitution experiments. Hence, assessing the toxicity of small molecule EXO1 inhibitors on BRCA1-deficient tumors, as well as BRCA1-proficient untransformed cells, should be prioritized in future studies. To potentially enlarge the clinical space in which EXO1 inhibitors could display beneficial effects, other HR-deficient settings beyond BRCA1-, BARD1-, and BRCA2-deficiency should be tested. Finally, our collective data indicate that SSA functions as an important DSB repair pathway in HR-deficient cells. However, mechanistic understanding of this pathway is far from complete and all described SSA factors are also involved in other genome maintenance pathways. A better understanding of this pathway would therefore greatly aid future studies on this DSB repair mechanism and its role in HR-deficient tumors.

STAR★METHODS

Detailed methods are provided in the online version of this paper and include the following:

- KEY RESOURCES TABLE
- RESOURCE AVAILABILITY
  - Lead contact
  - Materials availability
  - Data and code availability
- METHOD DETAILS
  - Cell lines
  - Plasmids and cloning
  - Viral transductions and transfections
  - Western blotting
  - Multicolor competition assay
  - Clonogenics
  - Cell Titer Glo assays
  - RNA isolation and qRT–PCR
  - Chromosomal aberrations
  - Micronuclei formation and yH2AX immunofluorescence
  - IR-induced foci immunofluorescence
  - PARylation analysis
  - S1 nuclease DNA fiber assay
  - DSB-spectrum assays
  - SSA at HBB locus
  - Clinical data analyses
  - Datasets
- QUANTIFICATION AND STATISTICAL ANALYSIS

SUPPLEMENTAL INFORMATION

Supplemental information can be found online at https://doi.org/10.1016/j.molcel.2023.12.039.

ACKNOWLEDGMENTS

We would like to thank Dr. Hiroyuki Sasanuma (Kyoto University, Japan) for sharing plasmids to generate BRCA1-mAID cells and Dr. Johan Staaf (Lund University, Sweden) for sharing expression data on triple-negative breast cancer cases. We also would like to thank Dr. Madalena Tarsounas (University of Oxford, UK) for sharing the H1299 pLKO^{TetOn} sh*BRCA2* cells, Dr. Neil Johnson (Fox Chase Cancer Center, USA) for sharing the MDA-MB-436 and MDA-MB-436 + BRCA1-WT cells, Dr. Ross Chapman (University of Oxford) for sharing the HCT116 BARD-AID cell line, and Dr. Stephen Elledge (Harvard University) for sharing the Human DLD1 WT and BRCA2-deficient cells. This work was funded by grants from the Dutch Research Council (NWO-VIDI grant #192.039 to S.M.N.; NWO-VICI grant #09150182110019 to M.A.T.M.v.V.), Oncode Institute (S.M.N.), Leiden University Medical Center (LUMC, MSCA-IF Seal of Excellence to B.v.d.K.), the Dutch Cancer Foundation (KWF, research grant #13472 to S.M.N. and H.v.A.; personal grant #BUIT 2015-7546 to B.v.d.K.), NIH (A.N.), NCI (contract HHSN2612015000031 to A.N.), the Ellison Medical Foundation (Senior Scholar in Aging Award AG-SS-2633-11 to A.N.), the Department of Defence (awards W81XWH-16-1-599 and W81XWH-19-10652 to A.N.), the Alex's Lemonade Stand Foundation (award to A.N.), and the European Research Council (Consolidator Grant STOP-FIX-GO #101043815 to M.S.L.). We thank Andrew Blackford for helpful discussions on this project. This publication and the underlying study have been made

possible partly based on data that Hartwig Medical Foundation has made available to the study through the Hartwig Medical Database.

AUTHOR CONTRIBUTIONS

The project was initiated by B.v.d.K. and S.M.N., and S.M.N. and H.v.A. supervised the project. Experiments were performed and analyzed by B.v.d.K., A.S., R.P., V.G., S.U., T.J.W., M.S.M.A., M.E., D.K., E. Callen, and S.M.N. and conceptualized by B.v.d.K., A.S., R.P., M.S.L., M.A.T.M.v.V., A.N., H.v.A., and S.M.N. *In silico* analyses of tumor material were performed and interpreted by B.v.d.K., A.v.H., J.B., H.M., E. Cuppen, and S.M.N. The manuscript was written by A.S. and S.M.N. with help from B.v.d.K., R.P., A.N., and H.v.A. and input from all other co-authors.

DECLARATION OF INTERESTS

M.A.T.M.v.V. has acted on the Scientific Advisory Boards of REPARE therapeutics and NODUS Oncology, unrelated to this work.

Received: March 16, 2023
Revised: October 14, 2023
Accepted: December 22, 2023
Published: January 23, 2024

REFERENCES

1. Nik-Zainal, S., Davies, H., Staaf, J., Ramakrishna, M., Glodzik, D., Zou, X., Martincorena, I., Alexandrov, L.B., Martin, S., Wedge, D.C., et al. (2016). Landscape of somatic mutations in 560 breast cancer whole-genome sequences. Nature *534*, 47–54.
2. Kandoth, C., McLellan, M.D., Vandin, F., Ye, K., Niu, B., Lu, C., Xie, M., Zhang, Q., McMichael, J.F., Wyczalkowski, M.A., et al. (2013). Mutational landscape and significance across 12 major cancer types. Nature *502*, 333–339.
3. Nguyen, L., W M Martens, J., Van Hoeck, A., and Cuppen, E. (2020). Pan-cancer landscape of homologous recombination deficiency. Nat. Commun. *11*, 5584.
4. Lord, C.J., and Ashworth, A. (2016). BRCAness revisited. Nat. Rev. Cancer *16*, 110–120.
5. Lord, C.J., and Ashworth, A. (2017). PARP inhibitors: synthetic lethality in the clinic. Science *355*, 1152–1158.
6. Noordermeer, S.M., and van Attikum, H. (2019). PARP inhibitor resistance: A tug-of-war in BRCA-mutated cells. Trends Cell Biol. *29*, 820–834.
7. Scully, R., Panday, A., Elango, R., and Willis, N.A. (2019). DNA double-strand break repair-pathway choice in somatic mammalian cells. Nat. Rev. Mol. Cell Biol. *20*, 698–714.
8. Zhao, W., Steinfeld, J.B., Liang, F., Chen, X., Maranon, D.G., Jian Ma, C., Kwon, Y., Rao, T., Wang, W., Sheng, C., et al. (2017). BRCA1-BARD1 promotes RAD51-mediated homologous DNA pairing. Nature *550*, 360–365.
9. Cruz-García, A., López-Saavedra, A., and Huertas, P. (2014). BRCA1 accelerates CtIP-mediated DNA-end resection. Cell Rep. *9*, 451–459.
10. Callen, E., Zong, D., Wu, W., Wong, N., Stanlie, A., Ishikawa, M., Pavani, R., Dumitrache, L.C., Byrum, A.K., Mendez-Dorantes, C., et al. (2020). 53BP1 enforces distinct pre- and post-resection blocks on homologous recombination. Mol. Cell *77*, 26–38.e7.
11. Chandramouly, G., Kwok, A., Huang, B., Willis, N.A., Xie, A., and Scully, R. (2013). BRCA1 and CtIP suppress long-tract gene conversion between sister chromatids. Nat. Commun. *4*, 2404.
12. Zhou, Y., Caron, P., Legube, G., and Paull, T.T. (2014). Quantitation of DNA double-strand break resection intermediates in human cells. Nucleic Acids Res. *42*, e19.
13. Nacson, J., Krais, J.J., Bernhardy, A.J., Clausen, E., Feng, W., Wang, Y., Nicolas, E., Cai, K.Q., Tricarico, R., Hua, X., et al. (2018). BRCA1 mutation-specific responses to 53BP1 loss-induced homologous recombination and PARP inhibitor resistance. Cell Rep. *25*, 1384.
14. Escribano-Díaz, C., Orthwein, A., Fradet-Turcotte, A., Xing, M., Young, J.T., Tkáč, J., Cook, M.A., Rosebrock, A.P., Munro, M., Canny, M.D., et al. (2013). A cell cycle-dependent regulatory circuit composed of 53BP1-RIF1 and BRCA1-CtIP controls DNA repair pathway choice. Mol. Cell *49*, 872–883.
15. Garcia, V., Phelps, S.E., Gray, S., and Neale, M.J. (2011). Bidirectional resection of DNA double-strand breaks by Mre11 and Exo1. Nature *479*, 241–244.
16. Gnügge, R., and Symington, L.S. (2021). DNA end resection during homologous recombination. Curr. Opin. Genet. Dev. *71*, 99–105.
17. Lu, H., Shamanna, R.A., Keijzers, G., Anand, R., Rasmussen, L.J., Cejka, P., Croteau, D.L., and Bohr, V.A. (2016). RECQL4 promotes DNA end resection in repair of DNA double-strand breaks. Cell Rep. *16*, 161–173.
18. Symington, L.S. (2016). Mechanism and regulation of DNA end resection in eukaryotes. Crit. Rev. Biochem. Mol. Biol. *51*, 195–212.
19. Misenko, S.M., Patel, D.S., Her, J., and Bunting, S.F. (2018). DNA repair and cell cycle checkpoint defects in a mouse model of 'BRCAness' are partially rescued by 53BP1 deletion. Cell Cycle *17*, 881–891.
20. Karanja, K.K., Cox, S.W., Duxin, J.P., Stewart, S.A., and Campbell, J.L. (2012). DNA2 and EXO1 in replication-coupled, homology-directed repair and in the interplay between HDR and the FA/BRCA network. Cell Cycle *11*, 3983–3996.
21. Kimble, M.T., Johnson, M.J., Nester, M.R., and Symington, L.S. (2023). Long-range DNA end resection supports homologous recombination by checkpoint activation rather than extensive homology generation. eLife *12*, e84322.
22. Tomimatsu, N., Mukherjee, B., Harris, J.L., Boffo, F.L., Hardebeck, M.C., Potts, P.R., Khanna, K.K., and Burma, S. (2017). DNA-damage-induced degradation of EXO1 exonuclease limits DNA end resection to ensure accurate DNA repair. J. Biol. Chem. *292*, 10779–10790.
23. van de Kooij, B., Kruswick, A., van Attikum, H., and Yaffe, M.B. (2022). Multi-pathway DNA-repair reporters reveal competition between end-joining, single-strand annealing and homologous recombination at Cas9-induced DNA double-strand breaks. Nat. Commun. *13*, 5295.
24. Patel, D.S., Misenko, S.M., Her, J., and Bunting, S.F. (2017). BLM helicase regulates DNA repair by counteracting RAD51 loading at DNA double-strand break sites. J. Cell Biol. *216*, 3521–3534.
25. Ochs, F., Somyajit, K., Altmeyer, M., Rask, M.B., Lukas, J., and Lukas, C. (2016). 53BP1 fosters fidelity of homology-directed DNA repair. Nat. Struct. Mol. Biol. *23*, 714–721.
26. Chen, C.C., Avdievich, E., Zhang, Y., Zhang, Y., Wei, K., Lee, K., Edelmann, W., Jasin, M., and LaRocque, J.R. (2017). EXO1 suppresses double-strand break induced homologous recombination between diverged sequences in mammalian cells. DNA Repair (Amst) *57*, 98–106.
27. Kelso, A.A., Lopezcolorado, F.W., Bhargava, R., and Stark, J.M. (2019). Distinct roles of RAD52 and POLQ in chromosomal break repair and replication stress response. PLoS Genet. *15*, e1008319.
28. Mateos-Gomez, P.A., Gong, F., Nair, N., Miller, K.M., Lazzerini-Denchi, E., and Sfeir, A. (2015). Mammalian polymerase theta promotes alternative NHEJ and suppresses recombination. Nature *518*, 254–257.
29. van Schendel, R., Romeijn, R., Buijs, H., and Tijsterman, M. (2021). Preservation of lagging strand integrity at sites of stalled replication by Pol alpha-primase and 9-1-1 complex. Sci. Adv. *7*, eabf2278.
30. Yousefzadeh, M.J., Wyatt, D.W., Takata, K., Mu, Y., Hensley, S.C., Tomida, J., Bylund, G.O., Doublié, S., Johansson, E., Ramsden, D.A., et al. (2014). Mechanism of suppression of chromosomal instability by DNA polymerase POLQ. PLoS Genet. *10*, e1004654.
31. Ceccaldi, R., Liu, J.C., Amunugama, R., Hajdu, I., Primack, B., Petalcorin, M.I., O'Connor, K.W., Konstantinopoulos, P.A., Elledge, S.J., Boulton, S.J., et al. (2015). Homologous-recombination-deficient tumours are dependent on Poltheta-mediated repair. Nature *518*, 258–262.

32. Feng, Z., Scott, S.P., Bussen, W., Sharma, G.G., Guo, G., Pandita, T.K., and Powell, S.N. (2011). Rad52 inactivation is synthetically lethal with BRCA2 deficiency. Proc. Natl. Acad. Sci. USA *108*, 686–691.

33. Lok, B.H., Carley, A.C., Tchang, B., and Powell, S.N. (2013). RAD52 inactivation is synthetically lethal with deficiencies in BRCA1 and PALB2 in addition to BRCA2 through RAD51-mediated homologous recombination. Oncogene *32*, 3552–3558.

34. Belan, O., Sebald, M., Adamowicz, M., Anand, R., Vancevska, A., Neves, J., Grinkevich, V., Hewitt, G., Segura-Bayona, S., Bellelli, R., et al. (2022). POLQ seals post-replicative ssDNA gaps to maintain genome stability in BRCA-deficient cancer cells. Mol. Cell *82*, 4664–4680.e9.

35. Mann, A., Ramirez-Otero, M.A., De Antoni, A., Hanthi, Y.W., Sannino, V., Baldi, G., Falbo, L., Schrempf, A., Bernardo, S., Loizou, J., and Costanzo, V. (2022). POLtheta prevents MRE11-NBS1-CtIP-dependent fork breakage in the absence of BRCA2/RAD51 by filling lagging-strand gaps. Mol. Cell *82*, 4218–4231.e8.

36. Schrempf, A., Bernardo, S., Arasa Verge, E.A., Ramirez Otero, M.A., Wilson, J., Kirchhofer, D., Timelthaler, G., Ambros, A.M., Kaya, A., Wieder, M., et al. (2022). POLtheta processes ssDNA gaps and promotes replication fork progression in BRCA1-deficient cells. Cell Rep. *41*, 111716.

37. Panzarino, N.J., Krais, J.J., Cong, K., Peng, M., Mosqueda, M., Nayak, S.U., Bond, S.M., Calvo, J.A., Doshi, M.B., Bere, M., et al. (2021). Replication gaps underlie BRCA deficiency and therapy response. Cancer Res. *81*, 1388–1397.

38. Paes Dias, M., Tripathi, V., van der Heijden, I., Cong, K., Manolika, E.M., Bhin, J., Gogola, E., Galanos, P., Annunziato, S., Lieftink, C., et al. (2021). Loss of nuclear DNA ligase III reverts PARP inhibitor resistance in BRCA1/53BP1 double-deficient cells by exposing ssDNA gaps. Mol. Cell *81*, 4692–4708.e9.

39. Cong, K., Peng, M., Kousholt, A.N., Lee, W.T.C., Lee, S., Nayak, S., Krais, J., VanderVere-Carozza, P.S., Pawelczak, K.S., Calvo, J., et al. (2021). Replication gaps are a key determinant of PARP inhibitor synthetic lethality with BRCA deficiency. Mol. Cell *81*, 3227.

40. Taglialatela, A., Leuzzi, G., Sannino, V., Cuella-Martin, R., Huang, J.W., Wu-Baer, F., Baer, R., Costanzo, V., and Ciccia, A. (2021). REV1-Polzeta maintains the viability of homologous recombination-deficient cancer cells through mutagenic repair of PRIMPOL-dependent ssDNA gaps. Mol. Cell *81*, 4008–4025.e7.

41. Adam, S., Rossi, S.E., Moatti, N., De Marco Zompit, M., Xue, Y., Ng, T.F., Álvarez-Quilón, A., Desjardins, J., Bhaskaran, V., Martino, G., et al. (2021). The CIP2A-TOPBP1 axis safeguards chromosome stability and is a synthetic lethal target for BRCA-mutated cancer. Nat. Cancer *2*, 1357–1371.

42. Álvarez-Quilón, A., Wojtaszek, J.L., Mathieu, M.C., Patel, T., Appel, C.D., Hustedt, N., Rossi, S.E., Wallace, B.D., Setiaputra, D., Adam, S., et al. (2020). Endogenous DNA 3′ blocks are vulnerabilities for BRCA1 and BRCA2 deficiency and are reversed by the APE2 nuclease. Mol. Cell *78*, 1152–1165.e8.

43. Bryant, H.E., Schultz, N., Thomas, H.D., Parker, K.M., Flower, D., Lopez, E., Kyle, S., Meuth, M., Curtin, N.J., and Helleday, T. (2005). Specific killing of BRCA2-deficient tumours with inhibitors of poly(ADP-ribose) polymerase. Nature *434*, 913–917.

44. Farmer, H., McCabe, N., Lord, C.J., Tutt, A.N., Johnson, D.A., Richardson, T.B., Santarosa, M., Dillon, K.J., Hickson, I., Knights, C., et al. (2005). Targeting the DNA repair defect in BRCA mutant cells as a therapeutic strategy. Nature *434*, 917–921.

45. Appanah, R., Jones, D., Falquet, B., and Rass, U. (2020). Limiting homologous recombination at stalled replication forks is essential for cell viability: DNA2 to the rescue. Curr. Genet. *66*, 1085–1092.

46. Hart, T., Tong, A.H.Y., Chan, K., Van Leeuwen, J., Seetharaman, A., Aregger, M., Chandrashekhar, M., Hustedt, N., Seth, S., Noonan, A., et al. (2017). Evaluation and design of genome-wide CRISPR/SpCas9 knockout screens. G3 (Bethesda) *7*, 2719–2727.

47. Lin, W., Sampathi, S., Dai, H., Liu, C., Zhou, M., Hu, J., Huang, Q., Campbell, J., Shin-Ya, K., Zheng, L., et al. (2013). Mammalian DNA2 helicase/nuclease cleaves G-quadruplex DNA and is required for telomere integrity. EMBO J. *32*, 1425–1439.

48. Noordermeer, S.M., Adam, S., Setiaputra, D., Barazas, M., Pettitt, S.J., Ling, A.K., Olivieri, M., Álvarez-Quilón, A., Moatti, N., Zimmermann, M., et al. (2018). The shieldin complex mediates 53BP1-dependent DNA repair. Nature *560*, 117–121.

49. Przetocka, S., Porro, A., Bolck, H.A., Walker, C., Lezaja, A., Trenner, A., von Aesch, C., Himmels, S.F., D'Andrea, A.D., Ceccaldi, R., et al. (2018). CtIP-mediated fork protection synergizes with BRCA1 to suppress genomic instability upon DNA replication stress. Mol. Cell *72*, 568–582.e6.

50. Buis, J., Wu, Y., Deng, Y., Leddon, J., Westfield, G., Eckersdorff, M., Sekiguchi, J.M., Chang, S., and Ferguson, D.O. (2008). Mre11 nuclease activity has essential roles in DNA repair and genomic stability distinct from ATM activation. Cell *135*, 85–96.

51. Polato, F., Callen, E., Wong, N., Faryabi, R., Bunting, S., Chen, H.T., Kozak, M., Kruhlak, M.J., Reczek, C.R., Lee, W.H., et al. (2014). CtIP-mediated resection is essential for viability and can operate independently of BRCA1. J. Exp. Med. *211*, 1027–1036.

52. Joukov, V., Chen, J., Fox, E.A., Green, J.B., and Livingston, D.M. (2001). Functional communication between endogenous BRCA1 and its partner, BARD1, during Xenopus laevis development. Proc. Natl. Acad. Sci. USA *98*, 12078–12083.

53. Elstrodt, F., Hollestelle, A., Nagel, J.H., Gorin, M., Wasielewski, M., van den Ouweland, A., Merajver, S.D., Ethier, S.P., and Schutte, M. (2006). BRCA1 mutation analysis of 41 human breast cancer cell lines reveals three new deleterious mutants. Cancer Res. *66*, 41–45.

54. Johnson, N., Johnson, S.F., Yao, W., Li, Y.C., Choi, Y.E., Bernhardy, A.J., Wang, Y., Capelletti, M., Sarosiek, K.A., Moreau, L.A., et al. (2013). Stabilization of mutant BRCA1 protein confers PARP inhibitor and platinum resistance. Proc. Natl. Acad. Sci. USA *110*, 17041–17046.

55. Tsukada, K., Jones, S.E., Bannister, J., Durin, M., Vendrell, I., Fawkes, M., Fischer, R., Kessler, B.M., Chapman, J.R., and Blackford, A.N. (2023). BLM and BRCA1-BARD1 coordinate complementary mechanisms of joint DNA molecule resolution. Mol. Cell *84*. https://doi.org/10.1016/j.molcel.2023.12.040.

56. Gottipati, P., Vischioni, B., Schultz, N., Solomons, J., Bryant, H.E., Djureinovic, T., Issaeva, N., Sleeth, K., Sharma, R.A., and Helleday, T. (2010). Poly(ADP-ribose) polymerase is hyperactivated in homologous recombination-defective cells. Cancer Res. *70*, 5389–5398.

57. Staaf, J., Glodzik, D., Bosch, A., Vallon-Christersson, J., Reutersward, C., Hakkinen, J., Degasperi, A., Amarante, T.D., Saal, L.H., Hegardt, C., et al. (2019). Whole-genome sequencing of triple-negative breast cancers in a population-based clinical study. Nat. Med. *25*, 1526–1533.

58. Knijnenburg, T.A., Wang, L., Zimmermann, M.T., Chambwe, N., Gao, G.F., Cherniack, A.D., Fan, H., Shen, H., Way, G.P., Greene, C.S., et al. (2018). Genomic and molecular landscape of DNA damage repair deficiency across the cancer genome atlas. Cell Rep. *23*, 239–254.e6.

59. Tarsounas, M., and Sung, P. (2020). The antitumorigenic roles of BRCA1-BARD1 in DNA repair and replication. Nat. Rev. Mol. Cell Biol. *21*, 284–299.

60. Xia, Y., Pao, G.M., Chen, H.W., Verma, I.M., and Hunter, T. (2003). Enhancement of BRCA1 E3 ubiquitin ligase activity through direct interaction with the BARD1 protein. J. Biol. Chem. *278*, 5255–5263.

61. Couch, F.J., Shimelis, H., Hu, C., Hart, S.N., Polley, E.C., Na, J., Hallberg, E., Moore, R., Thomas, A., Lilyquist, J., et al. (2017). Associations between cancer predisposition testing panel genes and breast cancer. JAMA Oncol. *3*, 1190–1196.

62. Becker, J.R., Clifford, G., Bonnet, C., Groth, A., Wilson, M.D., and Chapman, J.R. (2021). BARD1 reads H2A lysine 15 ubiquitination to direct homologous recombination. Nature *596*, 433–437.

63. Tang, M., Pei, G., Su, D., Wang, C., Feng, X., Srivastava, M., Chen, Z., Zhao, Z., and Chen, J. (2021). Genome-wide CRISPR screens reveal cyclin C as synthetic survival target of BRCA2. Nucleic Acids Res. *49*, 7476–7491.

64. Tacconi, E.M., Lai, X., Folio, C., Porru, M., Zonderland, G., Badie, S., Michl, J., Sechi, I., Rogier, M., Matía García, V., et al. (2017). BRCA1 and BRCA2 tumor suppressors protect against endogenous acetaldehyde toxicity. EMBO Mol. Med. *9*, 1398–1414.

65. Martínez-Jiménez, F., Movasati, A., Brunner, S.R., Nguyen, L., Priestley, P., Cuppen, E., and Van Hoeck, A. (2023). Pan-cancer whole-genome comparison of primary and metastatic solid tumours. Nature *618*, 333–341.

66. Keijzers, G., Bakula, D., Petr, M.A., Madsen, N.G.K., Teklu, A., Mkrtchyan, G., Osborne, B., and Scheibye-Knudsen, M. (2018). Human exonuclease 1 (EXO1) regulatory functions in DNA replication with putative roles in cancer. Int. J. Mol. Sci. *20*, 74.

67. Schlacher, K., Christ, N., Siaud, N., Egashira, A., Wu, H., and Jasin, M. (2011). Double-strand break repair-independent role for BRCA2 in blocking stalled replication fork degradation by MRE11. Cell *145*, 529–542.

68. Bunting, S.F., Callén, E., Wong, N., Chen, H.T., Polato, F., Gunn, A., Bothmer, A., Feldhahn, N., Fernandez-Capetillo, O., Cao, L., et al. (2010). 53BP1 inhibits homologous recombination in BRCA1-deficient cells by blocking resection of DNA breaks. Cell *141*, 243–254.

69. Bouwman, P., Aly, A., Escandell, J.M., Pieterse, M., Bartkova, J., van der Gulden, H., Hiddingh, S., Thanasoula, M., Kulkarni, A., Yang, Q., et al. (2010). 53BP1 loss rescues BRCA1 deficiency and is associated with triple-negative and BRCA-mutated breast cancers. Nat. Struct. Mol. Biol. *17*, 688–695.

70. Ray Chaudhuri, A., Callen, E., Ding, X., Gogola, E., Duarte, A.A., Lee, J.E., Wong, N., Lafarga, V., Calvo, J.A., Panzarino, N.J., et al. (2016). Replication fork stability confers chemoresistance in BRCA-deficient cells. Nature *535*, 382–387.

71. Lim, K.S., Li, H., Roberts, E.A., Gaudiano, E.F., Clairmont, C., Sambel, L.A., Ponnienselvan, K., Liu, J.C., Yang, C., Kozono, D., et al. (2018). USP1 is required for replication fork protection in BRCA1-deficient tumors. Mol. Cell *72*, 925–941.e4.

72. Quinet, A., Carvajal-Maldonado, D., Lemacon, D., and Vindigni, A. (2017). DNA fiber analysis: mind the gap! Methods Enzymol. *591*, 55–82.

73. Maréchal, A., and Zou, L. (2013). DNA damage sensing by the ATM and ATR kinases. Cold Spring Harb. Perspect. Biol. *5*, a012716.

74. Hanzlikova, H., and Caldecott, K.W. (2019). Perspectives on PARPs in S phase. Trends Genet. *35*, 412–422.

75. Eustermann, S., Wu, W.F., Langelier, M.F., Yang, J.C., Easton, L.E., Riccio, A.A., Pascal, J.M., and Neuhaus, D. (2015). Structural basis of detection and signaling of DNA single-strand breaks by human PARP-1. Mol. Cell *60*, 742–754.

76. Huang, D., and Kraus, W.L. (2022). The expanding universe of PARP1-mediated molecular and therapeutic mechanisms. Mol. Cell *82*, 2315–2334.

77. Kahli, M., Osmundson, J.S., Yeung, R., and Smith, D.J. (2019). Processing of eukaryotic Okazaki fragments by redundant nucleases can be uncoupled from ongoing DNA replication in vivo. Nucleic Acids Res. *47*, 1814–1822.

78. Qiu, J., Qian, Y., Chen, V., Guan, M.X., and Shen, B. (1999). Human exonuclease 1 functionally complements its yeast homologues in DNA recombination, RNA primer removal, and mutation avoidance. J. Biol. Chem. *274*, 17893–17900.

79. Hanzlikova, H., Kalasova, I., Demin, A.A., Pennicott, L.E., Cihlarova, Z., and Caldecott, K.W. (2018). The importance of poly(ADP-ribose) polymerase as a sensor of unligated Okazaki fragments during DNA replication. Mol. Cell *71*, 319–331.e3.

80. Vaitsiankova, A., Burdova, K., Sobol, M., Gautam, A., Benada, O., Hanzlikova, H., and Caldecott, K.W. (2022). PARP inhibition impedes the maturation of nascent DNA strands during DNA replication. Nat. Struct. Mol. Biol. *29*, 329–338.

81. García-de-Teresa, B., Rodríguez, A., and Frias, S. (2020). Chromosome instability in fanconi anemia: from breaks to phenotypic consequences. Genes (Basel) *11*, 1528.

82. Yu, V.P., Koehler, M., Steinlein, C., Schmid, M., Hanakahi, L.A., van Gool, A.J., West, S.C., and Venkitaraman, A.R. (2000). Gross chromosomal rearrangements and genetic exchange between nonhomologous chromosomes following BRCA2 inactivation. Genes Dev. *14*, 1400–1406.

83. Bhargava, R., Onyango, D.O., and Stark, J.M. (2016). Regulation of single-strand annealing and its role in genome maintenance. Trends Genet. *32*, 566–575.

84. Zhu, Z., Chung, W.H., Shim, E.Y., Lee, S.E., and Ira, G. (2008). Sgs1 helicase and two nucleases Dna2 and Exo1 resect DNA double-strand break ends. Cell *134*, 981–994.

85. Stark, J.M., Pierce, A.J., Oh, J., Pastink, A., and Jasin, M. (2004). Genetic steps of mammalian homologous repair with distinct mutagenic consequences. Mol. Cell. Biol. *24*, 9305–9316.

86. Prakash, R., Zhang, Y., Feng, W., and Jasin, M. (2015). Homologous recombination and human health: the roles of BRCA1, BRCA2, and associated proteins. Cold Spring Harb. Perspect. Biol. *7*, a016600.

87. Tutt, A., Bertwistle, D., Valentine, J., Gabriel, A., Swift, S., Ross, G., Griffin, C., Thacker, J., and Ashworth, A. (2001). Mutation in BRCA2 stimulates error-prone homology-directed repair of DNA double-strand breaks occurring between repeated sequences. EMBO J. *20*, 4704–4716.

88. Anantha, R.W., Simhadri, S., Foo, T.K., Miao, S., Liu, J., Shen, Z., Ganesan, S., and Xia, B. (2017). Functional and mutational landscapes of BRCA1 for homology-directed repair and therapy resistance. eLife *6*, e21350.

89. Wang, M., Li, W., Tomimatsu, N., Yu, C.H., Ji, J.H., Alejo, S., Witus, S.R., Alimbetov, D., Fitzgerald, O., Wu, B., et al. (2023). Crucial roles of the BRCA1-BARD1 E3 ubiquitin ligase activity in homology-directed DNA repair. Mol. Cell *83*, 3679–3691.e8.

90. Al-Zain, A.M., and Symington, L.S. (2021). The dark side of homology-directed repair. DNA Repair (Amst) *106*, 103181.

91. Tomimatsu, N., Mukherjee, B., Catherine Hardebeck, M., Ilcheva, M., Vanessa Camacho, C., Louise Harris, J., Porteus, M., Llorente, B., Khanna, K.K., and Burma, S. (2014). Phosphorylation of EXO1 by CDKs 1 and 2 regulates DNA end resection and repair pathway choice. Nat. Commun. *5*, 3561.

92. Setton, J., Hadi, K., Choo, Z.N., Kuchin, K.S., Tian, H., Da Cruz Paula, A., Rosiene, J., Selenica, P., Behr, J., Yao, X., et al. (2023). Long-molecule scars of backup DNA repair in BRCA1- and BRCA2-deficient cancers. Nature *621*, 129–137.

93. Densham, R.M., Garvin, A.J., Stone, H.R., Strachan, J., Baldock, R.A., Daza-Martin, M., Fletcher, A., Blair-Reid, S., Beesley, J., Johal, B., et al. (2016). Human BRCA1-BARD1 ubiquitin ligase activity counteracts chromatin barriers to DNA resection. Nat. Struct. Mol. Biol. *23*, 647–655.

94. Hoa, N.N., Kobayashi, J., Omura, M., Hirakawa, M., Yang, S.H., Komatsu, K., Paull, T.T., Takeda, S., and Sasanuma, H. (2015). BRCA1 and CtIP are both required to recruit Dna2 at double-strand breaks in homologous recombination. PLoS One *10*, e0124495.

95. Hale, A., Dhoonmoon, A., Straka, J., Nicolae, C.M., and Moldovan, G.L. (2023). Multi-step processing of replication stress-derived nascent strand DNA gaps by MRE11 and EXO1 nucleases. Nat. Commun. *14*, 6265.

96. Dhoonmoon, A., Nicolae, C.M., and Moldovan, G.L. (2022). The KU-PARP14 axis differentially regulates DNA resection at stalled replication forks by MRE11 and EXO1. Nat. Commun. *13*, 5063.

97. Lemaçon, D., Jackson, J., Quinet, A., Brickner, J.R., Li, S., Yazinski, S., You, Z., Ira, G., Zou, L., Mosammaparast, N., and Vindigni, A. (2017).

MRE11 and EXO1 nucleases degrade reversed forks and elicit MUS81-dependent fork rescue in BRCA2-deficient cells. Nat. Commun. *8*, 860.

98. Keijzers, G., Bohr, V.A., and Rasmussen, L.J. (2015). Human exonuclease 1 (EXO1) activity characterization and its function on flap structures. Biosci. Rep. *35*, e00206.
99. Lee, B.I., and Wilson, D.M., 3rd (1999). The RAD2 domain of human exonuclease 1 exhibits 5′ to 3′ exonuclease and flap structure-specific endonuclease activities. J. Biol. Chem. *274*, 37763–37769.
100. Mengwasser, K.E., Adeyemi, R.O., Leng, Y., Choi, M.Y., Clairmont, C., D'Andrea, A.D., and Elledge, S.J. (2019). Genetic screens reveal FEN1 and APEX2 as BRCA2 synthetic lethal targets. Mol. Cell *73*, 885–899.e6.
101. Sun, H., Ma, L., Tsai, Y.F., Abeywardana, T., Shen, B., and Zheng, L. (2023). Okazaki fragment maturation: DNA flap dynamics for cell proliferation and survival. Trends Cell Biol. *33*, 221–234.
102. Audebert, M., Salles, B., and Calsou, P. (2004). Involvement of poly(ADP-ribose) polymerase-1 and XRCC1/DNA ligase III in an alternative route for DNA double-strand breaks rejoining. J. Biol. Chem. *279*, 55117–55126.
103. Wang, M., Wu, W., Wu, W., Rosidi, B., Zhang, L., Wang, H., and Iliakis, G. (2006). PARP-1 and Ku compete for repair of DNA double strand breaks by distinct NHEJ pathways. Nucleic Acids Res. *34*, 6170–6182.
104. Truong, L.N., Li, Y., Shi, L.Z., Hwang, P.Y., He, J., Wang, H., Razavian, N., Berns, M.W., and Wu, X. (2013). Microhomology-mediated End Joining and Homologous Recombination share the initial end resection step to repair DNA double-strand breaks in mammalian cells. Proc. Natl. Acad. Sci. USA *110*, 7720–7725.
105. Vrtis, K.B., Dewar, J.M., Chistol, G., Wu, R.A., Graham, T.G.W., and Walter, J.C. (2021). Single-strand DNA breaks cause replisome disassembly. Mol. Cell *81*, 1309–1318.e6.
106. Cortés-Ledesma, F., and Aguilera, A. (2006). Double-strand breaks arising by replication through a nick are repaired by cohesin-dependent sister-chromatid exchange. EMBO Rep. *7*, 919–926.
107. Kuzminov, A. (2001). Single-strand interruptions in replicating chromosomes cause double-strand breaks. Proc. Natl. Acad. Sci. USA *98*, 8241–8246.
108. Simoneau, A., Xiong, R., and Zou, L. (2021). The trans cell cycle effects of PARP inhibitors underlie their selectivity toward BRCA1/2-deficient cells. Genes Dev. *35*, 1271–1289.
109. Novak, L.C., Chou, J., Colic, M., Bristow, C.A., and Hart, T. (2023). PICKLES v3: the updated database of pooled in vitro CRISPR knockout library essentiality screens. Nucleic Acids Res. *51*, D1117–D1121.
110. Gelot, C., Kovacs, M.T., Miron, S., Mylne, E., Haan, A., Boeffard-Dosierre, L., Ghouil, R., Popova, T., Dingli, F., Loew, D., et al. (2023). Poltheta is phosphorylated by PLK1 to repair double-strand breaks in mitosis. Nature *621*, 415–422.
111. Brambati, A., Sacco, O., Porcella, S., Heyza, J., Kareh, M., Schmidt, J.C., and Sfeir, A. (2023). RHINO directs MMEJ to repair DNA breaks in mitosis. Science *381*, 653–660.
112. Heijink, A.M., Stok, C., Porubsky, D., Manolika, E.M., de Kanter, J.K., Kok, Y.P., Everts, M., de Boer, H.R., Audrey, A., Bakker, F.J., et al. (2022). Sister chromatid exchanges induced by perturbed replication can form independently of BRCA1, BRCA2 and RAD51. Nat. Commun. *13*, 6722.
113. Llorens-Agost, M., Ensminger, M., Le, H.P., Gawai, A., Liu, J., Cruz-García, A., Bhetawal, S., Wood, R.D., Heyer, W.D., and Löbrich, M. (2021). POLtheta-mediated end joining is restricted by RAD52 and BRCA2 until the onset of mitosis. Nat. Cell Biol. *23*, 1095–1104.
114. de Jager, M., Dronkert, M.L., Modesti, M., Beerens, C.E., Kanaar, R., and van Gent, D.C. (2001). DNA-binding and strand-annealing activities of human Mre11: implications for its roles in DNA double-strand break repair pathways. Nucleic Acids Res. *29*, 1317–1325.
115. Schneider, C.A., Rasband, W.S., and Eliceiri, K.W. (2012). NIH Image to ImageJ: 25 years of image analysis. Nat. Methods *9*, 671–675.
116. Brinkman, E.K., Chen, T., Amendola, M., and van Steensel, B. (2014). Easy quantitative assessment of genome editing by sequence trace decomposition. Nucleic Acids Res. *42*, e168.
117. Sasanuma, H., Tsuda, M., Morimoto, S., Saha, L.K., Rahman, M.M., Kiyooka, Y., Fujiike, H., Cherniack, A.D., Itou, J., Callen Moreu, E., et al. (2018). BRCA1 ensures genome integrity by eliminating estrogen-induced pathological topoisomerase II-DNA complexes. Proc. Natl. Acad. Sci. USA *115*, E10642–E10651.
118. Sanjana, N.E., Shalem, O., and Zhang, F. (2014). Improved vectors and genome-wide libraries for CRISPR screening. Nat. Methods *11*, 783–784.
119. Ruffner, H., and Verma, I.M. (1997). BRCA1 is a cell cycle-regulated nuclear phosphoprotein. Proc. Natl. Acad. Sci. USA *94*, 7138–7143.
120. Bekker-Jensen, S., Lukas, C., Kitagawa, R., Melander, F., Kastan, M.B., Bartek, J., and Lukas, J. (2006). Spatial organization of the mammalian genome surveillance machinery in response to DNA strand breaks. J. Cell Biol. *173*, 195–206.
121. El-Shemerly, M., Janscak, P., Hess, D., Jiricny, J., and Ferrari, S. (2005). Degradation of human exonuclease 1b upon DNA synthesis inhibition. Cancer Res. *65*, 3604–3609.
122. Luijsterburg, M.S., de Krijger, I., Wiegant, W.W., Shah, R.G., Smeenk, G., de Groot, A.J.L., Pines, A., Vertegaal, A.C.O., Jacobs, J.J.L., Shah, G.M., and van Attikum, H. (2016). PARP1 links CHD2-mediated chromatin expansion and H3.3 deposition to DNA repair by non-homologous end-joining. Mol. Cell *61*, 547–562.
123. Li, Y., Roberts, N.D., Wala, J.A., Shapira, O., Schumacher, S.E., Kumar, K., Khurana, E., Waszak, S., Korbel, J.O., Haber, J.E., et al. (2020). Patterns of somatic structural variation in human cancer genomes. Nature *578*, 112–121.
124. Goldman, M.J., Craft, B., Hastie, M., Repečka, K., McDade, F., Kamath, A., Banerjee, A., Luo, Y., Rogers, D., Brooks, A.N., et al. (2020). Visualizing and interpreting cancer genomics data via the Xena platform. Nat. Biotechnol. *38*, 675–678.

CellPress
OPEN ACCESS

STAR★METHODS

KEY RESOURCES TABLE

REAGENT or RESOURCE	SOURCE	IDENTIFIER
Antibodies		
Mouse α 53BP1 (WB: 1:1,500)	Becton, Dickinson	# 612522; RRID: AB_399824
Rabbit α BARD1 (WB: 1:1,000)	Bethyl	A300-263A; RRID: AB_2061250
Rabbit α BLM (WB: 1:2,000)	Abcam	ab2179; RRID: AB_2290411
Mouse α BRCA1 (WB: 1:1,000)	Merck	OP92; RRID: AB_2750876
Rabbit α BRCA1 (WB: 1:2,000) (IF: 1:1,000)	Merck-Millipore	# 07-434; RRID: AB_2275035
Mouse α BRCA2 (WB: 1:1,000)	Merck	OP95; RRID: AB_2067762
Mouse α CHK1 (G-4) (WB: 1:1,000)	Santa-Cruz	sc-8408; RRID: AB_627257
Rabbit α pCHK1 (WB: 1:1,000)	Cell Signaling Technology	# 2348S
Mouse α CTIP (WB: 1:1,000)	Merck-Millipore	MABE1060
Rabbit α ERCC1 (WB: 1:500)	Santa-Cruz	sc-10785; RRID: AB_2278022
Rabbit α ERCC1 (WB: 1:1,000)	Cell Signaling Technology	# 3885
Rabbit α EXO1 (WB: 1:1,000)	Abcam	ab9506
Rabbit α EXO1 (WB: 1:1,000)	GeneTex	GTX109891; RRID: AB_11172320
Rabbit α EXO1 (WB: 1:1,000)	Merck-Millipore	ABE1354
Rabbit α GAPDH (WB: 1:5,000)	Sigma Aldrich	G9545; RRID: AB_796208
Rabbit α GAPDH (WB: 1:10,000)	Abcam	ab128915
Mouse α GFP (WB: 1:1,000)	Sigma Aldrich	# 11814460001; RRID: AB_390913
Rabbit α MRE11 (WB: 1:3,000)	De Jager et al.[114]	N/A
Rabbit α PALB2 (WB: 1:1,000)	Gift of Cristopher Fry	N/A
Mouse α TUBULIN (WB: 1:5,000)	Sigma Aldrich	T6199; RRID: AB_477583
Mouse α Ty1 (WB: 1:1,000)	Diagenode	C15200054
Mouse α RAD52 (WB: 1:100)	Santa-Cruz	sc-365341; RRID: AB_10851346
Rabbit α RAD52 (WB: 1:1,000)	Protein-tech	28045-1-AP; RRID: AB_2881046
Mouse α HSP90 (WB: 1:5,000)	Santa-Cruz	sc-131119
Mouse α XPF (WB: 1:300)	Santa-Cruz	sc-136153; AB_2098034
Goat α Mouse IgG IRDye 680 (WB: 1:15,000)	LI-COR	# 926-68070; RRID: AB_10956588
Goat α Mouse IgG IRDye 800 (WB: 1:15,000)	LI-COR	# 926-32210; RRID: AB_621842
Goat α Rabbit IgG IRDye 680 (WB: 1:15,000)	LI-COR	# 926-68071; RRID: AB_10956166
Goat α Rabbit IgG IRDye 800 (WB: 1:15,000)	LI-COR	# 926-32211; RRID: AB_621843
Goat α Mouse IgG HRP-labelled (WB: 1:5,000)	ThermoFisher Scientific	# 31432; RRID: 228302
Donkey α Rabbit IgG HRP-labelled (WB: 1:5,000)	ThermoFisher Scientific	# 31458; RRID: AB_228213
Goat α Rabbit IgG HRP-labelled (WB: 1:10,000)	Agilent	P0448; RRID: AB_2617138
Rabbit α Mouse IgG HRP-labelled (WB: 1:10,000)	Agilent	P0260; RRID: AB_2636929
Rabbit α PAR (IF: 1:500)	Trevigen	# 4336; RRID: AB_2721257
Rabbit α PAR (IF: 1:250)	Millipore	MABE1016; RRID: AB_2665466
Mouse α RPA32 (IF: 1:1,000)	Abcam	ab2175; RRID: AB_302873
Rat α RPA32 (IF: 1:1,000)	Cell Signaling	# 2208; RRID: AB_2238543

(*Continued on next page*)

Continued

REAGENT or RESOURCE	SOURCE	IDENTIFIER
Rabbit α RAD51 (IF: 1:15,000)	Bio-Academia	70-001
Mouse α yH2AX (pSer139; IF: 1:5,000)	Millipore	05-636; RRID: AB_309864
Goat α Mouse IgG AlexaFluor 488 (IF: 1:1,000)	ThermoFisher Scientific	A-11029; RRID: AB_2535804
Goat α Mouse IgG AlexaFluor 647 (IF: 1:1,000)	ThermoFisher Scientific	A-21235; RRID: AB_2535804
Goat α Rabbit IgG AlexaFluor 488 (IF: 1:1,000)	ThermoFisher Scientific	A-11034; RRID: AB_2576217
Goat α Rabbit IgG AlexaFluor 647 (IF: 1:1,000)	ThermoFisher Scientific	A-21245; RRID: AB_2535813
Chicken α Rat IgG AlexaFluor 488 (IF: 1:1,000)	ThermoFisher Scientific	A-21470; RRID: AB_2535873
Chemicals, peptides, and recombinant proteins		
Auxin	Sigma Aldrich	I3750-5G-A
PARG inhibitor	Tocris	PDD 00017273
CldU	Merck	C6891
EdU	Invitrogen	A10044
IdU	Merck	# I7125
S1 nuclease	Invitrogen	# 18001016
Azide-AlexaFluor 647	Invitrogen	A10277
Experimental models: Cell lines		
DLD1 cells	Gift from Dr. S. Elledge	N/A
H1299 pLKO^{TetOn} shBRCA2	Gift from Dr. M. Tarsounas	N/A
HCT116 BARD-AID	Gift from Dr. R. Chapman	N/A
HEK293T cells	ATCC	CRL-3216
HEK293T DSB-spectrum_V1	Van de Kooij et al.[23]	N/A
HEK293T DSB-spectrum_V3	van de Kooij et al.[23]	N/A
Mouse Embryonic Fibroblasts	Callen et al.[10]	N/A
MDA-MB-436 (+/- BRCA1 complementation)	Gift from Dr. N. Johnson	N/A
RPE1 hTERT cells	ATCC	CRL-4000
Oligonucleotides		
See Table S1	This paper	N/A
Recombinant DNA		
pLentiCRISPR_v2	Addgene	# 52961
pLentiGuide_eGFP	Noordermeer et al.[48]	N/A
pLentiGuide_mCherry	Noordermeer et al.[48]	N/A
pCW57.1	Addgene	# 41393
pLKO-1	Dharmacon/ Horizon	RHS4080
pRSITEP-U6Tet-sh-EF1-TetRep-2A-Puro	Cellecta	SVSHU6T16-L
pSpCas9-2A-iRFP670	van de Kooij et al.[23]	N/A
pMDLg/pRRE	Addgene	# 12251
pRSV-Rev	Addgene	# 12253
pMD2.G	Addgene	# 12259
Vectors to obtain endogenous BRCA1-mAID tag	Gift from Dr. H. Sasanuma	N/A
Software and algorithms		
ImageJ	Schneider et al.[115]	https://imagej.net/ij/index.html
Graphpad Prism	GraphPad Software	N/A

(*Continued on next page*)

Continued

REAGENT or RESOURCE	SOURCE	IDENTIFIER
Zen	Zeiss	N/A
Other		
Triple negative breast cancer cohort	Staaf et al.[57]	N/A
Breast cancer cohort	Nik-Zainal et al.[1]	N/A
Breast cancer cohort	TCGA	https://xenabrowser.net/datapages/?cohort=GDC%20TCGA%20Breast%20Cancer%20(BRCA)&removeHub=https%3A%2F%2Fxena.treehouse.gi.ucsc.edu%3A443
PAN-cancer cohort	Martinez-Jimenez et al.[65]	N/A

RESOURCE AVAILABILITY

Lead contact

Further information and requests for resources and reagents should be directed to and will be fulfilled by the lead contact, Sylvie Noordermeer (s.m.noordermeer@lumc.nl).

Materials availability

Newly generated materials are made available upon request by contacting the lead contact.

Data and code availability

- All raw data and uncropped western blots are available at Mendeley Data (https://doi.org/10.17632/zn77xfkyzw.1).
- This paper does not report original code.
- Any additional information required to reanalyse the data reported in this paper is available from the lead contact upon request.

METHOD DETAILS

Cell lines

RPE1 hTERT TP53$^{-/-}$ + FLAG-Cas9 (referred to as WT in this manuscript), RPE1 hTERT TP53$^{-/-}$ *BRCA1*$^{-/-}$ + FLAG-Cas9 (referred to as *BRCA1*$^{-/-}$ in this manuscript), RPE1 hTERT *TP53*$^{-/-}$ *BRCA1*$^{-/-}$ *53BP1*$^{-/-}$ + FLAG-Cas9 cells (referred to as *BRCA1*$^{-/-}$ *53BP1*$^{-/-}$ in this manuscript) were previously described.[48] RPE1 hTERT cells were obtained from ATCC (Manassas, VA, USA). RPE1 hTERT *PAC*$^{-/-}$ *TP53*$^{-/-}$ (referred to as WT in this manuscript) and RPE1 hTERT *PAC*$^{-/-}$ *TP53*$^{-/-}$ *BRCA1*$^{-/-}$ (referred to as *BRCA1*$^{-/-}$ in this manuscript) cells were generated by nucleofection of pLentiCRISPR_v2 containing the following sgRNAs: sg*PAC*: ACGCGCGTCGGGCTCGACAT; sg*TP53*: CAGAATGCAAGAAGCCCAGA; sg*BRCA1*: AAGGGTAGCTGTTAGAAGGC. Subsequently, cells were clonally expanded and genotyping was performed by PCR amplification and Sanger sequencing of the targeted locus, followed by TIDE analysis.[116]

The BRCA1 gene in RPE1 hTERT *PAC*$^{-/-}$ *TP53*$^{-/-}$ cells was endogenously C-terminally tagged with *mAID-GFP* as previously described[117] (referred to as *BRCA1-mAID* in this manuscript). RPE1 hTERT *TP53*$^{-/-}$ *BRCA1-mAID-GFP EXO1*$^{-/-}$ cells (referred to as *EXO1*$^{-/-}$ in this manuscript) were obtained by nucleofection with pLentiCRISPR_v2 containing sg*EXO1* (GCGTGGGAT TGGATTAGCAA) and subsequent clonal selection and genotyping as aforementioned. To deplete AID-tagged BRCA1, cells were treated with 500 μM auxin (Sigma Aldrich, Saint Louis, MO, USA; stock solution 35 mg/mL in EtOH) for 48 hours, unless stated otherwise.

HEK 293T cells were obtained from ATCC (Manassas, VA, USA) and HEK 293T DSB-Spectrum_V3 cells were previously described.[23] H1299 pLKO^{TetOn} sh*BRCA2* cells (gift from Dr. Madalena Tarsounas) were previously described.[64] HCT116 BARD1-AID (gift from Dr. Ross Chapman) were previously described.[62] RPE1, HEK 293T, H1299 and HCT116 cells were cultured in Dulbecco's Modified Eagle's Medium (DMEM, high glucose, GlutaMAX™ and pyruvate supplemented (ThermoFisher Scientific, Waltham, MA, USA)) + 10% Fetal Calf Serum (FCS) and 1% penicillin + streptomycin (Pen-Strep).

MDA-MB-436 and MDA-MB-436+BRCA1WT cells (gift from Dr. Neil Johnson) and were cultured in Roswell Park Memorial Institute (RPMI) 1640 supplemented with 10% heat-inactivated FCS (Gemini Bio-Products, West Sacramento, CA, USA) and 1% Pen-Strep (ThermoFisher Scientific). Mouse embryonic fibroblasts (MEFs) were previously generated as described in[10] and were cultured in DMEM (ThermoFisher Scientific) supplemented with 10% FCS + 1% Pen-Strep. Human DLD-1 WT and *BRCA2*$^{-/-}$ cells (gift from Dr. Stephen Elledge) were maintained in RPMI-1640 Medium (ATCC modification) supplemented with 10% heat-inactivated FCS and 1% Pen-Strep.

All cells were maintained at 37°C, 5% CO_2. When BRCA1-deficient, cells were maintained at 37°C, 5% CO_2, 3% O_2 unless stated otherwise.

Plasmids and cloning

All purification of plasmid DNA or PCR products was done using commercially available kits (Qiagen, Hilden, Germany) according to the manufacturer's protocol. For the multi-colour competition assays, the sgRNAs targeting the described genes were cloned into the BsmBI-digested lentiviral expression construct pLentiGuide-GFP.[48] For other experimental purposes, these same sgRNAs were cloned into BsmBI-digested pLentiCRISPR_v2[118] or BpiI-digested pSpCas9-2A-iRFP670.[23] See Table S1 for used sgRNA sequences. To obtain pCW57.1-BRCA1-3xTy1, full-length BRCA1 was PCR-amplified from pCL-MFG-BRCA1 (Addgene #12341[119]) with a triple Ty1-tag included in the reverse primer and subsequently cloned into pENTR_1A and transferred to pCW57.1 using gateway cloning. RAD52 was PCR amplified from pEYFP-RAD52 (gift from Jiri Lukas[120]) and cloned into pDONR221-eGFP to obtain an eGFP-RAD52 fusion, followed by a gateway LR reaction for transfer into pCW57.1. hEXO1 was PCR amplified from pTXB1-EXO1b (Addgene #68267[121]) and transferred directly into pCW57.1 using Gibson Assembly. hEXO1^{D173A} mutation in the pCW57.1 vector was obtained with site-directed mutagenesis.

For EXO1 knockdown using shRNA, human targeting sh*EXO1* (see Table S1 for sequence, TRC Lentiviral shRNA cloned in pLKO.1, Dharmacon) was used for MDA-MB-436 and mouse targeting sh*EXO1* (see Table S1 for sequence, cloned in pRSITEP-U6Tet-sh-EF1-TetRep-2A-Puro from Cellecta Catalog #: SVSHU6T16-L) was used for MEFs.

Viral transductions and transfections

Lentivirus was produced in HEK 293T cells by jetPEI transfection (Polyplus Transfection, Illkirch, France) or X-tremeGENE 9 DNA Transfection Reagent (Sigma) of a pLenti, pCW57.1, or shRNA plasmid with third generation packaging vectors pMDLg/pRRE, pRSV-Rev and pMD2.G. Viral supernatants were harvested 48-72 hours post transfection, filtered (0.45 μm filter) and used to transduce cells at an MOI of ~ 1 in the presence of 4 μg/mL or 10 μg/mL polybrene. For RPE1 cells, 10-15 μg/mL puromycin was used for selection, for RPE1 *PAC*$^{-/-}$ cells, 2 μg/mL of puromycin was used, for MDA-MB-436 and DLD1 cells 3 μg/mL puromycin was used, and for HCT116 cells 0.5-1 μg/mL puromycin was used. Transfections with siRNAs were performed using Lipofectamine RNAiMAX (Invitrogen, Carlsbad, CA, USA) according to the manufacturer's protocol (see Table S1 for used siRNAs). 16 hours post transfection, the medium was refreshed. Cells transfected with siRNAs were used for experiments 48-72 hours after transfection. Lipofectamine 2000 (Invitrogen, Carlsbad, CA, USA) was used according to manufacturer's instructions for transfection of cDNA into HEK 293T DSB-Spectrum_V3 cells.

Western blotting

Cells were lysed in RIPA lysis buffer (1% NP-40, 50 mM Tris-HCl pH 7.5, 150 mM NaCl, 0.1% SDS, 3 mM $MgCl_2$, 0.5% sodium deoxycholate) supplemented with Complete Protease Inhibitor Cocktail (Sigma Aldrich) and 100 U/mL Benzonase (Sigma Aldrich). LDS or SDS sample buffer with DTT was added to the lysates, followed by denaturation at 95°C for 5 minutes. Proteins were separated by SDS-PAGE on 4-12 % gradient gels (ThermoFisher Scientific) or 4%–15% Criterion TGX pre-cast midi protein gel (Bio-Rad, Hercules, CA, USA) and transferred to Amersham Protran premium 0.45 μm nitrocellulose membrane (GE Healthcare Life Sciences, Chicago, IL, USA). Membranes were blocked with 5% skimmed milk (Santa Cruz Biotechnology, Dallas, TX, USA) in 1x TBS or Blocking buffer for fluorescent WB (Rockland, Pottstown, PA, USA), and stained with primary and secondary antibodies. After secondary antibody-staining, the membranes were imaged on an Odyssey CLx scanner (LI-COR BioSciences, Milton, UK), followed by image analysis using ImageStudio (LI-COR BioSciences). Alternatively, when HRP-labelled secondary antibodies were used the membranes were treated with the WesternBright ECL HRP Substrate kit (Advansta, San Jose, CA, USA) and imaged on an Amersham Imager 680 (Bioké, Leiden, The Netherlands).

Multicolor competition assay

RPE1 WT or RPE1 BRCA1$^{-/-}$ + FLAG-Cas9 cells were transduced with viral supernatants of pLenti-Guide-GFP containing a sgRNA (see Table S1 for sequences) for the gene of interest (GOI_sgRNA) or pLenti-Guide-mCherry-LacZ_sgRNA. Transduced cells were selected by puromycin treatment for 48h (15 μg/mL for RPE1 WT cells; 10 μg/mL for RPE1 *BRCA1*$^{-/-}$ cells), and subsequently, GFP- and mCherry-positive cells were mixed 1:1. Mixed populations were seeded at 10,000 cells per well in a 12-well plate and imaged every 3 days for a total of 18 days using an ArrayScan Cellomics high content microscope (Thermo Fisher Scientific). HCS Studio Cell Analysis Software (Thermo Fisher Scientific) was used to quantify the number of GFP- and mCherry-positive cells per well. Cells were passaged upon confluency. To assess gene editing efficiencies of the used sgRNAs, whole cell lysates were isolated 5 days post transduction and assessed by western blotting for the targeted proteins.

Clonogenics

RPE1 hTERT, H1299 and HCT116 cells were seeded in 10-cm dishes (RPE1 WT or RPE1 BRCA1$^{-/-}$ complemented with BRCA1-WT: 250 cells, RPE1 *BRCA1*$^{-/-}$: 1,000-1,500 cells, RPE1 *BRCA1*$^{-/-}$ *53BP1*$^{-/-}$: 500 cells, RPE1 *BRCA1-mAID*: 500 cells, H1299 pLKO^{TetOn} sh*BRCA2*: 500 cells, HCT116 BARD1-AID: 4,000 cells) and treated as indicated. Medium containing Olaparib (16 nM or 50 nM) (Selleck Chemicals, Planegg, Germany), doxycycline (1 μg/mL) or auxin (500 μM) was refreshed after 7 days. After 14 days, colonies

were stained with crystal violet (0.4 % (w/v) crystal violet, 20% methanol) and counted manually. HCT116 BARD1-AID cells were treated with doxycycline (2 μg/mL), auxin (1 mM) was added after 24 hours, refreshed after 7 days and colonies were stained after 10 days.

For Figure S7B, DLD1 WT or BRCA2$^{-/-}$ cells were lentivirally infected to express Cas9 and an sgRNA targeting *AAVS1* (control), *RAD52* (sgRNA #1), *XPF* (sgRNA #2) or *ERCC1* (sgRNA #2), followed by selection using puromycin (1 μg/mL). At 5-7 days after infection, cells were plated in 6-wells plates, 2,000 cells per well, allowed to proliferate for 10-14 days, and subsequently fixed and stained in 0.2% Coomassie Brilliant Blue (Bio-Rad) solution containing 50% methanol (Merck) and 14% acetic acid (Merck).

Cell Titer Glo assays

To analyze cell growth and cell viability after EXO1 depletion, MDA-MB-436 and MDA-MB-436+BRCA1WT, DLD1 WT and *BRCA2*$^{-/-}$ cells were transduced with virus containing the sg*EXO1* construction and plated in 6-well plates (10,000 cells per well per sample) after Puromycin selection. Similarly, WT and BRCA1 MEF cells were plated at a density of 10,000 cells per well and doxycycline (1 μg/mL) was added to induce sh*EXO1* expression. The medium was replenished every 3 days and cells were sub cultured when confluent. Cell viability was measured after 12 days using CellTiter-Glo Luminescent Cell Viability Assay (Promega, Madison, WI, USA) following manufacturer's instructions.

RNA isolation and qRT–PCR

Total RNA was extracted from cells using Trizol Reagent (Invitrogen), and cDNA was made using SuperScript II Reverse Transcriptase (ThermoFisher), according to manufacturer's instructions. qPCR was performed using iTaq Universal SyBR Green (Bio-Rad). Samples were run and analyzed on a Bio-Rad CFX96 Real-Time PCR detection system. Primer sequences: m*EXO1* forward: 5′ TGTTCGACCCCATCCAAAGG 3′ and m*EXO1* reverse: 5′ GTACTGCCCAGCGTAAGTCA 3′.

Chromosomal aberrations

Colcemid (0.1 μg/mL) was added to cells at 80% confluency 3 hours prior to harvesting. Cells were harvested by trypsinization and normal medium was added to quench trypsin before centrifugation (5 minutes, 1000 rpm). Supernatant was removed and normal medium was added to create a cell suspension. Freshly made hypotonic solution (1:1 0.4% Na-citrate: 0.4% KCl) was added dropwise to the cell suspension (14:1). Cells were centrifuged 8 minutes, 800 rpm, supernatant was removed partially whereafter 2.5 mL freshly made fixative (3:1 MeOH: Acetic Acid) was added dropwise. Following three washes with the fixative, cells were taken up in fresh fixative. Fixed cells were spread with a Pasteur pipet onto a cleaned microscope slide pre-wet with fixative. Another drop of fixative was added onto the slide with the spread cells at a 45 degrees angle and air-dried overnight. Spreads were stained and mounted using VECTASHIELD® Antifade Mounting Medium with DAPI (Vector Laboratories, Newark, CA, USA). Pictures were made using a Zeiss Axio Imager 2 fluorescent microscope (Zeiss, Oberkochen, Germany) at a 63x zoom. All slides were blinded before quantification of the chromosomal aberrations. At least 40 metaphase spreads per condition per replicate were analyzed.

Micronuclei formation and yH2AX immunofluorescence

Cells were grown in glass bottom 96 well plates (Greiner, Kremsmünster, Austria) until 85% confluency and fixed with 2% (w/v) paraformaldehyde (Sigma Aldrich) in PBS for 20 minutes, washed three times with PBS, and permeabilized with 0.3% Triton X-100 (Sigma Aldrich) in PBS for 20 minutes. Permeabilized cells were subsequently washed three times with PBS and blocked with PBS^{+} (5 g/L BSA (Sigma Aldrich) and 1.5 g/L glycine (Sigma Aldrich) in PBS) for 30 minutes. Blocked cells were incubated 1.5 hours with anti-BRCA1 or anti-yH2AX in PBS^{+}, washed 4 times with PBS, and incubated 1 hour with 5 μg/mL Hoechst 34580 (stock 5 mg/mL in H_2O) (Thermo Fisher) and anti-mouse Alexa 647 in PBS^{+}.

To measure yH2AX in EdU positive cells, the cells were incubated 30 minutes at 37°C with EdU (10 μM, stock solution 40 mM) (Invitrogen) before fixation. After staining with the primary and secondary antibody as described above, the cells were fixed with 2% (w/v) paraformaldehyde in PBS for 5 minutes and washed twice with PBS. Subsequently, the fixed cells were incubated with click-it reaction mix (100 mM Tris-HCl pH 8.5, 10 μM Azide-Alexa 647, 1 mM $CuSO_4$ and 100 mM Ascorbic acid (Sigma Aldrich) added lastly) for 30 min at room temperature.

Cells were washed again 4 times with PBS and analysed using the CellInsight CX7 LZR High content Analysis Platform (Thermo Fisher). For the micronuclei formation, 200 cells per condition per replicate were imaged and the micronuclei were quantified manually. For endogenous yH2AX foci formation 2,000 cells per condition per replicate were imaged and the average nuclear intensity per cell was quantified by the CellInsight CX7 LZR High content Analysis Platform.

IR-induced foci immunofluorescence

For RPA IRIF, RAD51 IRIF and RAD52 IRIF cells were grown on sterile 13 mm glass coverslips till 85% confluency and fixed 3 hours after irradiation with 10 Gy. Cells were pre-extracted with ice cold nuclear extraction (NuEx) buffer (20 mM Hepes pH 7.5, 20 mM NaCl, 5 mM $MgCl_2$, 1 mM DTT, 0.5% NP-40 (IGEPAL CA-630, Sigma Aldrich), 1x Complete Protease Inhibitor Cocktail (Sigma Aldrich) for 12 minutes at 4°C and directly fixed with 2% (w/v) paraformaldehyde in PBS (20 minutes at room temperature). For RAD51 IRIF, cells were grown on sterile 13 mm glass coverslips till 85% confluency and fixed 3 hours after irradiation with 10 Gy. Cells were fixed and

permeabilized with 1% (w/v) paraformaldehyde, 0.5% Triton X-100 in PBS for 20 minutes at room temperature, washed three times with PBS, further fixed and permeabilized with 1% (w/v) paraformaldehyde, 0.3% Triton X-100 in PBS for 20 minutes.

Subsequently, the fixed and permeabilized cells were washed three times with PBS and blocked with PBS^+ as described above for 30 minutes at room temperature. Blocked cells were incubated 1.5 hours with the primary antibody in PBS^+, washed 4 times with PBS, and incubated 1 hour with DAPI 0.1 μg/mL (stock 100 μg/mL) and the secondary antibody in PBS^+. All antibody incubations were performed at room temperature. After washing 4 times with PBS the coverslips were mounted using Aqua-Poly/mount (Polysciences, Warrington, PA, USA). Pictures were made using the Zeiss Axio Imager 2 fluorescent microscope at a 40x zoom. Foci of at least 100 cells per condition per replicate were quantified using the IRIF analysis 3.2 Plugin in ImageJ.[122]

PARylation analysis

For the analysis of PAR levels in EdU-positive MDA-MB-436 or DLD1 cells, cells were plated on coverslips pre-treated with 0.1% Gelatin in 6-well plates. Cells were then incubated with EdU for 30 minutes and PARGi (Tocris, Bristol, UK) for 20 minutes before collection. Subsequently, cells were pre-extracted (20 mM Hepes, 50 mM NaCl, 3 mM $MgCl_2$, 0.3 M sucrose, 0.2% Triton X-100) on ice for 5 minutes, fixed with 4% paraformaldehyde (Electron Microscopy Sciences, Hatfield, PA, USA) for 10 minutes and permeabilized using 0.5% Triton X-100 for 10 minutes. The fixed and permeabilized cells were blocked and incubated with the appropriate primary, secondary antibody and click-it reaction for EdU as aforementioned. Images were captured at 40x zoom on a Lionheart LX automated microscope (BioTek, Winooski, VT, USA) or at 63x zoom with an Axio Cam MRC5 attached to an Axio Observer Z1 epifluorescence microscope (Zeiss). Quantification of total nuclear intensity was performed using the Gen5 spot analysis software (BioTek).

S1 nuclease DNA fiber assay

Cells were labeled with 25 μM 5-chloro-2'-deoxyuridine (CldU, Merck) for 15 minutes, washed three times with PBS and followed by a second label with 250 μM 5-iodo-2'-deoxyuridine (IdU, Merck) for 1 h. Cells were then permeabilized with CSK buffer (100 mM NaCl, 10 mM PIPES pH 6.8, 300 mM sucrose, 3mM $MgCl_2$, 0.5% Triton-X) for 10 minutes at RT, then incubated with S1 nuclease buffer (30 mM sodium acetate pH 4.6, 10 mM zinc acetate, 5% glycerol and 50 mM NaCl) with or without 20 U/mL S1 nuclease (Invitrogen) for 30 minutes at 37°C. The nuclei were then collected in PBS with 0.1% BSA with cell scraper and pelleted at 7000 rpm for 5 minutes at 4°C and resuspended in PBS. 2 μL of the cell suspension were spotted on a positively charged slide (VWR) and then mixed with 7 μL of lysis buffer (200 mM Tris-HCl pH 7.4, 50 mM EDTA, 0.5% (w/v) SDS). The cells were incubated in lysis buffer horizontally for 5 min and then tilted at ~ 45° allowing the drop to run by gravity. The DNA spreads were air-dried at RT and were then fixed in methanol/acetic acid (3:1) at RT for 10 min and stored at 4°C O/N. Slides were rehydrated by rinsing with 1x PBS three times, DNA was denatured with 2.5 M HCl for 1 h at RT, and slides were washed four times with 1x PBS. Slides were blocked in 2% BSA in 1x PBS/0.1% Tween-20 (PBST) for 1 h in dark at RT. Slides were stained with primary antibodies diluted in blocking buffer (Rat α CldU (Abcam clone BU1/75; 1:200), Mouse α IdU (Bectone Dickinson clone B44; 1:100) for 2 h at RT in dark, washed three times with PBST and then incubated with 2% PFA for 10 min, and washed again three times with PBST. Slides were then incubated with secondary antibodies diluted in blocking buffer (α Rat Alexa Fluor 555; 1:400 and α Mouse Alexa Fluor 488; 1:400) for 1 h in dark at RT and were washed three times with PBST and one time with blocking buffer. Slides were air-dried for 1 h and were mounted with Aqua-poly/mount (Brunschwig, Amsterdam, The Netherlands). Slides were conserved at 4°C in dark until imaging. Fibers were visualized and imaged using the Zeiss Axio Imager 2 fluorescent microscope at a 40x zoom. Imaged were recorded and analysed with ZEN 2012 (Blue edition, Version 1.1.0.0) software and analyzed in Image J (1.48v).

DSB-spectrum assays

HEK 293T DSB-Spectrum_V3 cells were seeded and transfected with siRNAs the next day. A second siRNA transfection was performed 24 hours after the first transfection. 6-8 hours after the second siRNA transfection, 20,000 cells were seeded per well in 96-well plates. 24 hours post-seeding, the cells were transfected in technical duplicate with pX459-Cas9-sgRNA-iRFP construct containing either sg*BFP* targeting DSB-Spectrum or sg*AAVS1*. The cells were trypsinised and analysed by flow cytometry 48-96 hours after the DSB-Spectrum targeting transfection. FlowJo software (BD Biosciences, Franklin Lakes, NJ, USA) was used to analyze the acquired flow cytometry data. To select the live, single cell population gating on forward and side-scatter was applied. Subsequently sg*AAVS1* or sg*BFP* targeted cells were selected by gating on iRFP. On this population gating was applied to quantify the frequencies of BFP-/mCherry-, BFP-/mCherry+ and GFP+ cells. The frequency of each fluorescent sub-population in the sg*AAVS1*-transfected cells was subtracted from the frequency of that same population in the sg*BFP*-transfected cells. The resulting background-corrected frequencies were normalized to the si*CTRL* transfected cells.

To generate EXO1, RAD52, XPF or ERCC1 depleted cell-lines in the HEK 293T DSB-Spectrum_V3 background, cells were transfected with pSpCas9-2A-iRFP670 plasmids containing *AAVS1*-targeting control sgRNA, or an sgRNA (in all cases sgRNA #1, see Table S1) targeting the gene-of-interest. Next, cells were sorted on high iRFP670 expression and expanded for 7-10 days. To generate the EXO1 KO cells, single cell clones were expanded from this sg*EXO1* pool.

SSA at HBB locus

HEK293T DSB-Spectrum_V3 cells, either sg*AAVS1* control, or sg*EXO1* cells, were reverse transfected with siRNA by plating 200,000 cells per well in 12-well plates on top of siRNA transfection mixes. At 48h after plating, transfection medium was replaced with fresh medium, and cells were transfected with pSpCas9-2A-Blasticidin plasmid containing *HBB*-targeting sgRNA. Cells were harvested 32-48h post cDNA transfection, and genomic DNA was extracted using the PureLink Genomic DNA mini kit (Invitrogen) according to manufacturer's instructions. Next 200 ng genomic DNA was added as template for a PCR reaction using HBB SSA FWD primer (5′-AACAGCCAATCTCAGGGCAA-3′) and HBB SSA REV primer (5′-CACTGACCTCCCACATTCCC3′) and LongAmp Taq DNA polymerase (New England Biolabs) according to manufacturer's instructions. Cycling parameters were adapted to include a 65-60°C annealing temperature touchdown PCR of five cycles (-1°C per cycle), followed by 25 cycles annealing at 59°C. PCR products were analyzed by DNA gel electrophoresis.

Clinical data analyses

Correlations between *EXO1* and *BLM* expression and *BRCA1*- or *BRCA2*-mutations was studied in three cancer cohorts. The first cohort contained 247 patients diagnosed with triple-negative breast cancer of which 22 tumours harboured biallelic *BRCA1*-mutations and 59 tumours displayed *BRCA1* promotor hypermethylation.[57] The second contained 342 patients diagnosed with breast cancer of which 15 tumours harboured deleterious *BRCA1*-mutations.[1] The third cohort consisted of a unified whole genome mutational dataset of the Hartwig Medical Foundation (Hartwig) and the Pan-Cancer Analysis of Whole Genomes (PCAWG).[65] HR-status was classified according to genome analysis using the CHORD algorithm as previously described,[3] identifying 35 tumours with a BRCA1-type HR-defective signature and 72 tumours with a BRCA2-type HR-defective signature. This cohort was also used to identify SSA signatures by structural variants (SV) calling using the genomic rearrangement toolkit LINX (https://doi.org/10.1016/j.xgen.2022.100112). This tool integrates copy number profiles and the SV calls from PURPLE (https://doi.org/10.1038/s41586-019-1689-y) and GRIDSS (https://doi.org/10.1186/s13059-021-02423-x) that enables the characterization and annotation of simple and complex genomic rearrangements. Specifically, LINX chains one or more SVs and classifies these SV clusters into various event types ('ResolvedType'). We defined deletions and duplications as clusters with a ResolvedType of 'DEL' or 'DUP' whose start and end breakpoints were located on the same chromosome (*i.e.* intrachromosomal). Duplication or deletion events that were part of a complex SV event were excluded from this analysis as these are not induced by a continuous SV-related mutation process. Subsequently, each duplication or deletion event was annotated with its homology sequence length at the break junction using IHOMPOS from PURPLE. This SV mutation feature represents the imperfect homology length of a break junction left and right from the break-end and is calculated by performing local Smith-Waterman alignment of the breakpoint sequence to the reference sequence up to 300bps either side of the break junction. The total homology length of a break-end was calculated as the sum of the left and right IHOMPOS sequence length around the break-end. Lastly, the logics of the PCAWG SV reference paper[123] were used to classify SV scars. Duplication events were subsequently excluded from analysis, and all deletions bearing an (imperfect) homology sequence length longer than 10 or 50 bps were annotated as SSA mutation scars. The cut-off of 10 bps was chosen to rule out inclusion of NHEJ or alt-EJ scars, which are generally dependent on shorter stretches of homology.

To correlate expression levels to HR status, the Xena functional genomic platform[124] was used to extract both genome-wide gene expression levels (FPKM) as well as the HRD-score[58] for all samples in the TCGA breast cancer cohort. Tumour samples were excluded from analysis in case HRD-score and/or gene expression data were absent. If multiple tumour samples from a single patient were sequenced, as was the case for six patients, the expression values were averaged. Next, for each individual gene, the Pearson correlation coefficient between gene expression level and HRD score was determined.

Datasets

The Hartwig data was provided under data transfer agreement DR-247 from the Hartwig Medical Foundation. The PCAWG-US was approved by National Institutes of Health (NIH) for the dataset General Research Use in The Cancer Genome Atlas (TCGA) on 25 February 2021 under application number 100344-3. Access to the non-US PCAWG samples was granted via the Data Access Compliance Office (DACO) Application Number DACO-1050905 on 6 October 2017.

QUANTIFICATION AND STATISTICAL ANALYSIS

Information on the used statistical test, number of repeats and p values can be found in the figure legends.